2,7-Fluorene-bridged Complexes Containing Electroactive "Fe(η^5-C$_5$Me$_5$)(κ^2-dppe)C≡C-" Endgroups: Molecular Wires and Remarkable Nonlinear Electrochromes

Floriane Malvolti,[a] Cédric Rouxel,[b] Amédée Triadon,[a] Guillaume Grelaud,[a,c] Nicolas Richy,[a] Olivier Mongin,[a,b] Mireille Blanchard-Desce,[b,d] Loic Toupet,[e] Fazira I. Abdul Razak,[c] Robert Stranger,[c] Marek Samoc,[f,g] Adam Barlow,[c] Marie P. Cifuentes,[c] Mark G. Humphrey,[c,] and Frédéric Paul[a,*]*

[a] *Institut des Sciences Chimiques de Rennes* - UMR CNRS 6226 **-** Université de Rennes 1 - Campus de Beaulieu - Bât. 10C - 35042 Rennes Cedex (France).
[b] *Chimie et Photonique Moléculaire* - UMR CNRS 6510 **-** Université de Rennes 1 - Campus de Beaulieu - Bât. 10C - 35042 Rennes Cedex (France).
[c] *Research School of Chemistry*, Australian National University, Canberra, ACT 2601 (Australia).
[d] *Institut des Sciences Moléculaires* - UMR 5255 – Université de Bordeaux, 351 cours de la Libération, 33405 Talence (France).
[e] *Institut de Physique de Rennes (IPR)* - UMR CNRS 6251 **-** Université de Rennes I - Campus de Beaulieu - 35042 Rennes Cedex (France)
[f] *Laser Physics Centre*, *Research School of Physics and Engineering,* Australian National University, Canberra, ACT 0200 (Australia).
[g] *Advanced Materials Engineering and Modeling Group*, *Faculty of Chemistry,* Wroclaw University of Technology, 50370 Wroclaw (Poland).

Supporting Information Placeholder

ABSTRACT: The 2,7-fluorenyl-bridged Fe(η^5-C$_5$Me$_5$)(κ^2-dppe)[C≡C(2,7-C$_{13}$H$_6$/Bu$_2$)C≡C]Fe(η^5-C$_5$Me$_5$)(κ^2-dppe) (**1a**), its extended analogue Fe(η^5-C$_5$Me$_5$)(κ^2-dppe)[C≡C(1,4-C$_6$H$_4$)C≡C(2,7-C$_{13}$H$_6$/Bu$_2$)C≡C(1,4-C$_6$H$_4$)C≡C](η^5-C$_5$Me$_5$)(κ^2-dppe) (**1b**) and the corresponding mononuclear complexes Fe(η^5-C$_5$Me$_5$)(κ^2-dppe)[C≡C(2-C$_{13}$H$_7$/Bu$_2$)] (**2a**) and Fe(η^5-C$_5$Me$_5$)(κ^2-dppe)[C≡C(1,4-C$_6$H$_4$)C≡C(2-C$_{13}$H$_7$/Bu$_2$)] (**2b**), which model one half of these molecules, have been synthesized and characterized in their various redox states. The molecular wire characteristics of the dinuclear complexes were examined in their mixed-valent states, with progression from **1a**[PF$_6$] to **1b**[PF$_6$] resulting in a sharp decrease in electronic coupling. The cubic nonlinear optical properties of these species were investigated over the visible and near-IR range, a particular emphasis being set on their multiphoton absorption properties; the complexes are shown to function as redox-switchable nonlinear chromophores at selected wavelengths, and the more extended derivatives shown to exhibit the more promising NLO performance.

INTRODUCTION

The 2,7-fluorenyl unit, with its high fluorescence quantum yield[1] and large multi-photon absorption cross-sections,[2] was identified very early as an outstanding building block for the construction of molecules for electronic[3,4,5] and photonic[6] applications. For example, this unit has been incorporated in organic and organometallic (discrete or polymeric) structures designed for optoelectronics,[7] optical limiting[8,9] or bio-imaging.[10] In these applications, the central fluorenyl linker is most often functionalized at the 2,7-positions with unsaturated π-conjugated arms terminated by electron-releasing substituents.[11,12]

In a continuation of studies aimed at identifying efficient organoiron-based molecular wires,[13,14] we considered exploiting the electron-transfer properties of such a planar and conjugated unit in Fe(II)/Fe(III) dinuclear mixed valent (MV) alkynyl complexes featuring "Fe(η^5-C$_5$Me$_5$)(η^2-dppe)C≡C-" endgroups, such as **1a**$^+$ or **1b**$^+$ (Chart 1), with the related mononuclear complexes **2a-b**[PF$_6$]$_n$ (n = 0, 1)

potentially constituting useful molecular model complexes to enhance understanding of the electronic interactions between the metal center and the fluorenyl-based alkynyl ligands in a given redox state. In particular, the comparison of **1a**[PF$_6$] with its known (non-planar) 4,4'-biphenyl analogue (**3**[PF$_6$])[15] was expected to probe the likely beneficial effects of planarity of such a central unit in the spacer on the intramolecular electronic delocalization. As already disclosed in a communication,[16] an increase in the electronic coupling of the redox-active termini actually occurs in proceeding from **3**[PF$_6$] to **1a**[PF$_6$]. It was now clearly of interest to probe the electronic coupling in the extended derivative **1b**[PF$_6$].
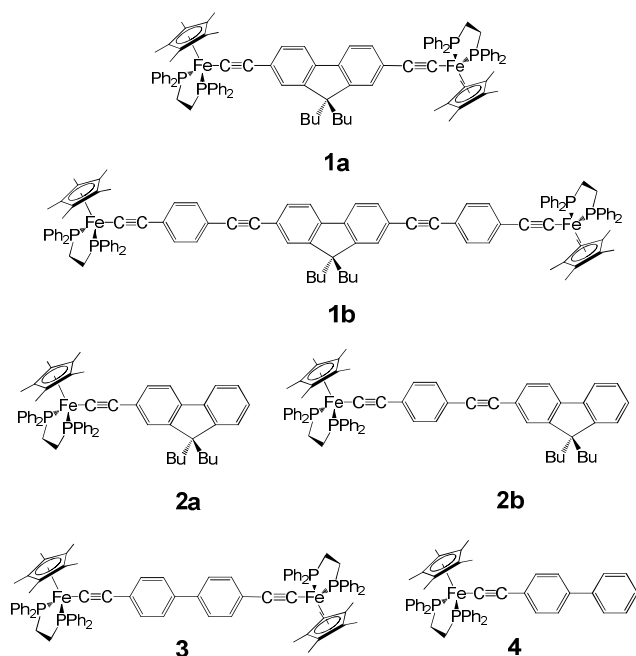

Chart 1. Selected Fluorenyl- and Biphenyl-based Organoiron Complexes.

Independent of these results, polynuclear organometallic architectures incorporating alkynyl complexes of d^6 metal centers have been shown to possess large cubic nonlinear optical (NLO) properties, particularly two-photon absorption (TPA), at specific wavelengths.[17] The NLO application potential of d^6 metal alkynyl complexes identified in these earlier studies,[18] coupled to the electron-releasing capability

previously established for the organoiron "Fe(η^5-C$_5$Me$_5$)(η^2-dppe)C≡C-" group,[19] encouraged us to study the absorptive NLO behavior of **1a-b** in their various redox-states (Chart 1).[20] Indeed, these Fe(II) complexes constitute organometallic analogues of known organic fluorene derivatives functionalized by donor groups in the 2,7-positions that often possess large TPA cross-sections.[2,11,12]

Furthermore, because such organoiron alkynyl complexes are usually stable (and isolable) in their cationic Fe(III) state,[14] a redox state in which the electron-releasing power of the organometallic end-group should be strongly diminished, we also wondered if redox-tuneable NLO-active molecules would result from the combination of this particular organometallic fragment and 2,7-diethynylfluorene, similar to observations with related homometallic and heterometallic alkynyl complexes.[20] This is anticipated at wavelengths where strong TPA occurs because TPA is related to the imaginary part of the cubic molecular polarizability (γ_{imag}), and γ_{imag} is usually influenced by a change in the donor capability of the nearby metal center, as can also be inferred from the perturbation expression often derived to express γ (eq 1).[20,21] From this expression, one can readily see that changes in the linear absorption spectrum (wavelengths of maxima, extinction coefficients/oscillator strengths of charge-transfer bands) brought about by the (reversible) oxidation of the metal center in these compounds should in turn strongly modify their cubic NLO properties, particularly at wavelengths where strong TPA takes place.

$$\gamma \propto -\mu_{ge}^4/E_{ge}^3 + \mu_{ge}^2\mu_{ee'}^2/E_{ge}^2E_{ge'} + \mu_{ge}^2(\mu_{ee} - \mu_{gg})^2/E_{ge}^3$$
(1)

Several electrochromic metal-alkynyl-functionalized fluorenes have been reported,[22] but few possess electron-rich redox-active metals, and, to the best of our knowledge, none thus far incorporate this particular organoiron endgroup.[23,24] We report herein the synthesis and characterization of the Fe(II) complexes **1a-b** and **2a-b** and of their various oxidized states. We also report studies on the intramolecular electron-transfer in the MV complexes **1a-b**[PF$_6$], studies of the cubic NLO properties of **3**, **4** and all new derivatives by Z-scan, linear optical properties assessed by absorption and emission

2

spectrometry, and DFT studies rationalizing the experimental observations. The results from the present studies are compared to those for related organometallic structures, and the potential of these complexes for electrochemical switching of cubic NLO properties is briefly discussed.

RESULTS
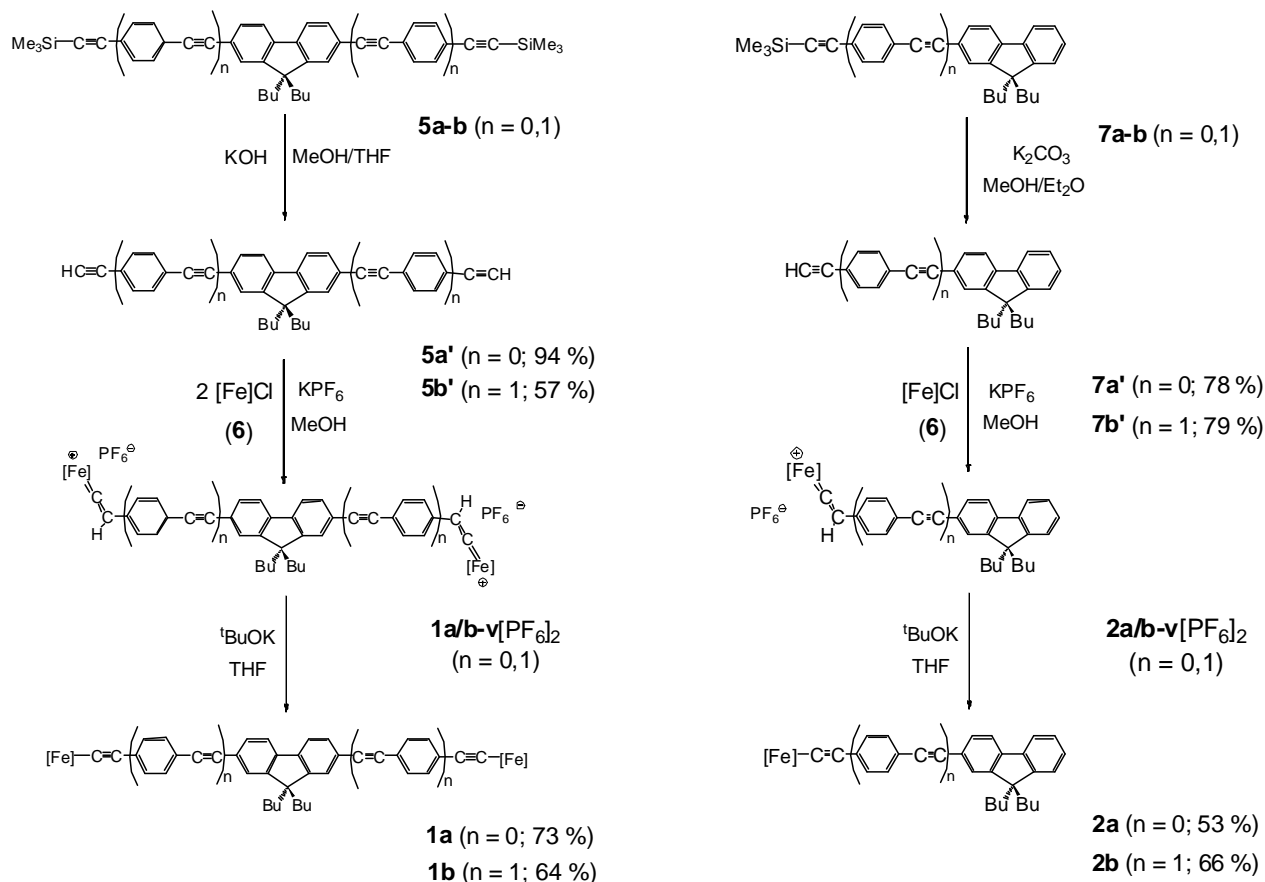
Scheme 1. Synthesis of the Fe(II) Complexes 1a-b and 2a-b ([Fe] = Fe(η^5-C$_5$Me$_5$)(κ^2-dppe)).

Synthesis and Characterization of the Fe(II) Complexes. The target dinuclear Fe(II) alkynyl complexes **1a-b** and **2a-b** were synthesized from the organic diyne precursors of the bridge (**5a'-b'**) and the Fe(II) chloride precursor **6**, following a classic two step alkyne activation reaction (Scheme 1).[15,25] The two butyl groups at the 9-position of the fluorene group were installed to ensure sufficient solubility of the resulting

complexes. Mono- and bis-vinylidene complexes **1a/b-v** and **2a/b-v** were formed as intermediates during these syntheses and, in the case of **1a-v[PF$_6$]$_2$** and **2a-v[PF$_6$]**, were briefly characterized by ^{31}P NMR spectroscopy. The ligands **5a'-b'** and **7a'-b'** were generated from their trimethylsilyl-protected precursors (**5a-b** and **7a-b**), which were themselves synthesized in a similar fashion to related compounds and fully characterized (Supporting Information).[23,26]

The orange/red complexes **1a/b** and **2a/b** were extensively characterized.[14] The presence of the triple bond(s) was confirmed in all cases by the observation of the corresponding $\nu_{C\equiv C}$ modes (Table 1). The identity of these stretching modes was further confirmed by Raman spectroscopy: because of their more pseudo-symmetric environments, internal alkynes give rise to much stronger signals in the Raman spectra than terminal alkynes.[27] In addition, small red crystals were

3

grown from toluene-pentane or C_6H_6-pentane mixtures for **1a, 2a** and **2b** (Figure 1).

Table 1. IR Data for Selected Complexes in CH$_2$Cl$_2$ Solutions^a (cm^{-1}).

Cmpd	Fe(II)	Fe(II)/Fe(III)	Fe(III)	$\Delta\nu_{C\equiv C}$ ^{b}	Ref.
	$\nu_{C\equiv C}$	$\nu_{C\equiv C}$	$\nu_{C\equiv C}$	Fe(II)/Fe(III)	
1a	2041	2030/1966	1983	-58	this work
1b	2045	2045/1993	1993	-52	this work
		1954 (sh)	1953 (sh)		
	2193 ^{c}	2195	2194 ^{c}	+1	
2a	2041	/	1985	-56	this work
2b	2045	/	1992	-53	this work
	2194 ^{c}		2196 ^{c}	+2	
3	2051	2043/1979	1991	-60	15
4	2051	/	1991	-61	15

^{a} Solid-state $\nu_{C\equiv C}$ values obtained in KBr for these complexes are given in the Experimental Section. ^{b} Fe(II) vs. Fe(III) $\nu_{C\equiv C}$ difference (PF$_6^-$ counter ion). ^{c} Very weak peak.

Solid-state Structures of 1a, 2a and 2b. The solid-state structures of **1a**, **2a** and **2b** were determined. The dinuclear compound **1a** (Figure 1a) crystallizes in the orthorhombic symmetry group P_{bca}, with one molecule in the asymmetric unit and one benzene molecule as solvate (see Experimental Section). The two butyl chains at the 9 and 9' positions of the fluorenyl group are slightly disordered, but the key geometric parameters of the molecule could nevertheless be obtained with good accuracy. The two metal centers feature piano-stool coordination spheres with the usual angles and distances for Fe(II) centers.[25,28,29] The structure of the dinuclear complex **1a** possesses a perfectly planar carbon-rich bridge that adopts a gauche structure relative to the two Fe-Cp* centroid axes in the solid state. This contrasts with the previously reported biphenyl analogue **3** (Chart 1), in which the bridge is apparently coplanar and roughly perpendicular to the two Fe-Cp* centroids.[15] The gauche conformation in **1a** is possibly induced in the solid state by the steric bulk of the two butyl chains at the 9 and 9' positions. The fluorenyl bridge imposes an intramolecular Fe-Fe mean distance of

15.9 Å, while the through-space Fe-Fe distance with the five nearest neighbouring molecules is slightly shorter in the crystal (9.2-11.9 Å). This intramolecular Fe-Fe distance is an important structural feature for evaluating the electronic coupling (H_{FeFe}) in the corresponding MV complex **1a**[PF$_6$].[16] Overall, these distances are similar to those previously found for **3** (16.2 Å).[15]
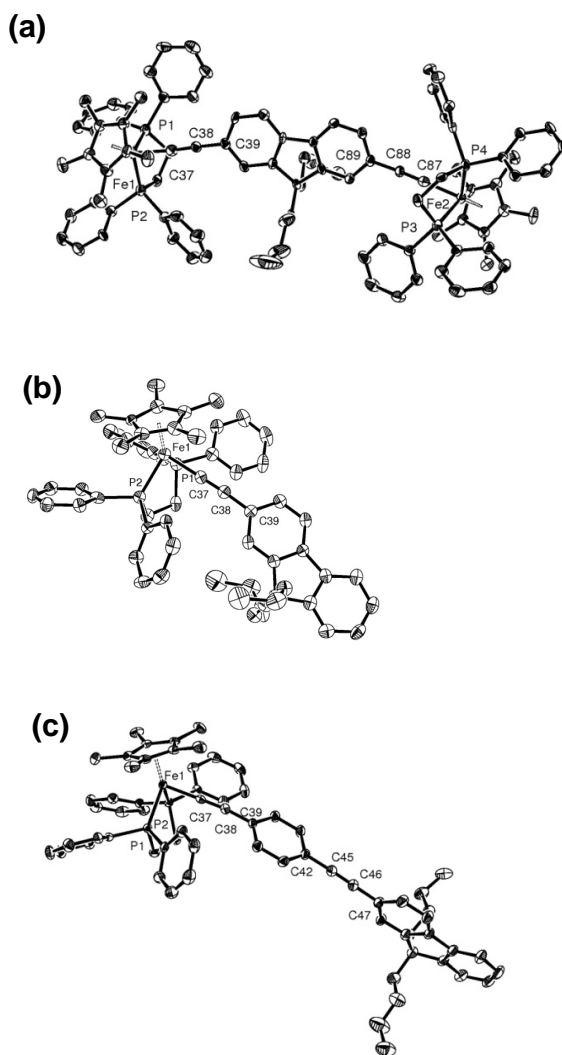

Figure 1. ORTEP representations of **1a** (a)**, 2a** (b) and **2b** (c) at the 50% probability level. Selected distances (Å) and angles (deg): (a) Fe1-(Cp*)$_{centroid}$ 1.753, Fe1-P1 2.1930(12), Fe1-P2 2.1977(11), Fe1-C37 1.889(4), C37-C38 1.233(5), C38-C39 1.452(5), P1-Fe1-P2 86.19(4), Fe1-C37-C38 171.6(3), C37-C38-C39 178.1(4), (Cp*)$_{centroid}$-Fe1-C39-C40 −54.5, Fe2-(Cp*)$_{centroid}$ 1.758, Fe2-P3 2.1910(12), Fe2-P4 2.2156(10), Fe2-C87 1.913(4), C87-C88 1.236(5), C88-C89 1.449(5), Fe2-C87-C88 179.8(4), C87-C88-C89 174.3(4), P3-Fe2-P4

4

85.60(4), (Cp*)$_{centroid}$-Fe2-C89-C90 −120.8; (b) Fe1-(Cp*)$_{centroid}$ 1.740, Fe1-P1 2.1788(15), Fe1-P2 2.1874(15), Fe1-C37 1.902(5), C37-C38 1.205(6), C38-C39 1.434(7), P1-Fe1-P2 86.06(6), Fe1-C37-C38 179.0(4), C37-C38-C39 176.0(5), (Cp*)$_{centroid}$-Fe1-C39-C40 −66.7; (c) Fe1-(Cp*)$_{centroid}$ 1.736, Fe1-P1 2.1904(6), Fe1-P2 2.1725(6), Fe1-C37 1.893(2), C37-C38 1.220(3), C38-C39 1.436(3), C42-C45 1.444(3), C45-C46 1.194(3), C46-C47 1.442(3), P1-Fe1-P2 86.05(2), Fe1-C37-C38 179.4(2), C37-C38-C39 173.2(2), (Cp*)$_{centroid}$-Fe1-C39-C40 108.7, C41-C42-C47-C48 -75.5.

The mononuclear complexes **2a-b** (Figures 1b-c) crystallize in the monoclinic groups P2$_1$/n and C2/c, respectively, with **2b** possessing one disordered toluene solvate in the asymmetric unit (Experimental Section). The bond distances and angles are again as expected for piano-stool Fe(II) arylalkynyl moieties and similar to those previously observed for **4** (Chart 1).[25,28,29] A conformation where the first aryl group is approximately "parallel" to the mean C$_5$Me$_5$ plane is observed with the alkynyl ligand of **2b**, but the fluorenyl mean plane lies nearly perpendicular to it, with a C41-C42-C47-C48 torsion angle of -75.5°; such a twisted conformation is likely induced by cell packing so as to minimize steric interactions.

Cyclic Voltammetry Studies. Cyclic voltammograms (CVs) were recorded for **1a-b** and **2a-b** (Table 2). While the CV of **2a** in CH$_2$Cl$_2$ reveals a chemically reversible one-electron process at - 0.17 V, the CV of **1a** exhibits two weakly separated waves at ca. -0.11 and -0.22 V *vs*. SCE, corresponding to the stepwise Fe(II)/Fe(III) oxidations of each organometallic endgroup. These systems appear chemically reversible at a scan rate of 0.1 V/s, the separation between the redox potentials (111 ± 3 mV) being accurately derived by fitting the voltammograms at various scanning speeds (Supporting Information).

$$(RT/F)\log(K_c) = \Delta E° \qquad (2)$$

As previously discussed,[16] based on eq. 2, this corresponds to a thermodynamic equilibrium constant (K_c) of 76 (± 8) for the comproportionation reaction between the homovalent Fe(II)/Fe(II) (**1**) and Fe(III)/Fe(III) species (**1**[PF$_6$]$_2$) at 25 °C (Scheme 2).[30,31] This indicates that the MV complex **1a**[PF$_6$]

will not exist in a "pure" state in solution at ambient temperature, but will always equilibrate with non-negligible amounts of its homovalent "parents" **1a** and **1a**[PF$_6$]$_2$. In contrast, the two one-electron metal-centered oxidations of **1b** are not resolved in the CV, occurring at a similar potential value to that of the mononuclear complex **2b** (-0.12 V). This demonstrates that the **1b**/**1b**$^{2+}$ comproportionation equilibrium constant is lower than for **1a**$^+$ and lies closer to the value corresponding to a statistical distribution (i.e. K_c = 4).[30] In addition to these chemically reversible metal-centered processes, an irreversible process is observed near 1.3 V or 1.4 V for **1a**/**2a** or **1b**/**2b**, respectively, likely corresponding to the oxidation of the fluorene group.[4]

Table 2. Electrochemical Data for Complexes 1a-b & 2a-b.

Cmpd	E^0 ($\Delta E_p{}^a$)	ΔE^0	i_c/i_a	Ref.
1a	- 0.11 (0.06) $^{b, c}$	0.11 ^{d}	1	**16**
	- 0.22 (0.06) $^{b, c}$		1	
2a	- 0.17 (0.08)	/	1	this work
1b	- 0.12 (0.08)	< 0.06	1	this work
2b	- 0.12 (0.08)	/	1	this work
3	- 0.11 (0.06) $^{b, c}$	0.06	1	**15**
	- 0.17 (0.06) $^{b, c}$		1	
4	-0.16 (0.07)	/	1	**15**

All E° values are in V vs. SCE. Conditions (unless stated otherwise): CH$_2$Cl$_2$ solvent, 0.1 M [NBu$_4$][PF$_6$] supporting electrolyte, 20 °C, Pt electrode, sweep rate 0.1 V s^{-1}. Ferrocene/ferrocenium (FcH/FcH$^+$) was used as an internal reference for potential measurements. ^{a} Difference between cathodic and anodic peak potentials. ^{b} Au electrode instead of Pt, sweep rate 0.2 V s^{-1}. ^{c} Values extracted by simulation. ^{d} 84 mV in acetone.[16]

Synthesis and Characterization of the Corresponding Fe(III) Complexes. The Fe(III) complexes **1a-b**[PF$_6$]$_2$ and **2a-b**[PF$_6$] were isolated following chemical oxidation with one and two equivalents of ferrocenium hexafluorophosphate, respectively (Scheme 2). They were characterized by infrared, NMR and ESR spectroscopy, while cyclic voltammetry confirmed the parentage of the neutral complexes **1a-b** and **2a-b**.
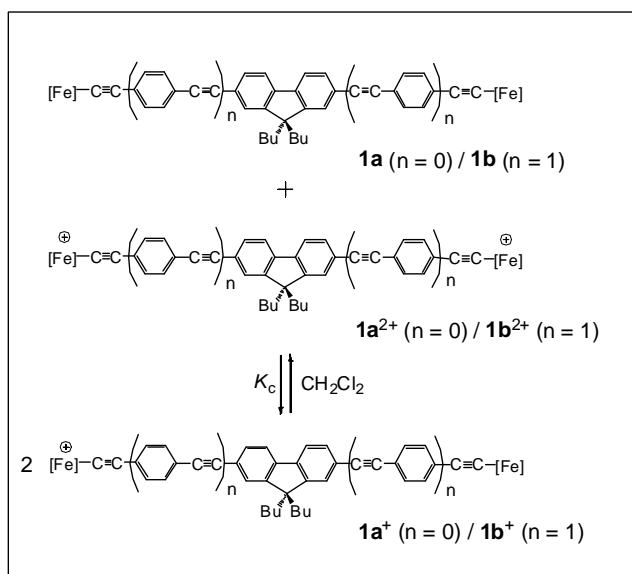
5
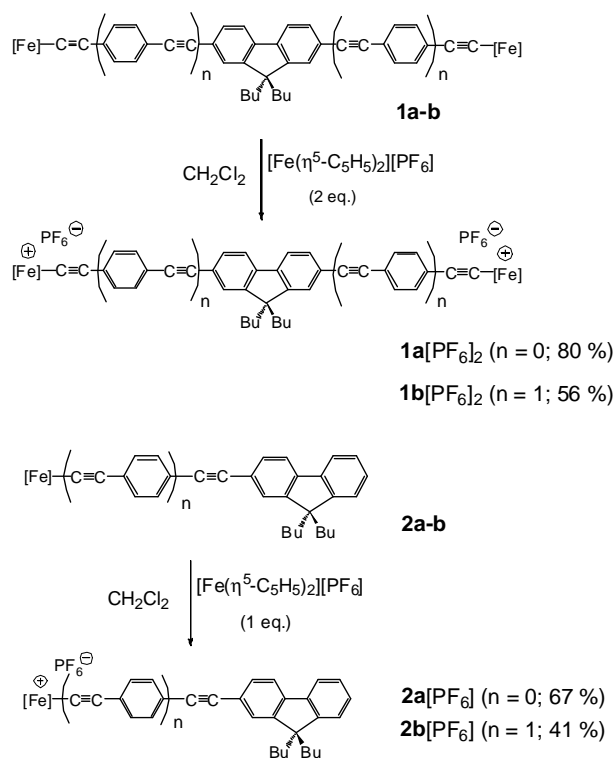
Scheme 2. Comproportionation Reactions between 1a/1b and 1a[PF₆]₂/1b[PF₆]₂ (Inset) and Synthesis of the Fe(III) Complexes 1a-b[PF₆]₂ and 2a-b[PF₆] ([Fe] = Fe(η^5-C₅Me₅)(κ^2-dppe)).

Table 3. ESR Spectra for Compounds in Frozen CH₂Cl₂/1,2-C₂H₄Cl₂ Solutions at 80 K.

Cmpd	g_1	g_2	g_3	Δg	Ref.
1a⁺	2.380	2035	1.984	0.397	[16]
1a²⁺		2.25			this work
	2.426 [a]	2.035 [a]	1.981 [a]		
2a⁺	2.425	2.034	1.980	0.445	this work
1b⁺	2.410	2.025	1.980	0.430	
1b²⁺		2.23			
2b⁺	2.473	2.029	1.973	0.500	this work
3²⁺		2.035			[15]
4⁺	2.439	2.032	1.975	0.464	[15]

[a] *Signal for pure solid sample of 1a²⁺ (no signal corresponding to a hypothetical forbidden $\Delta m_S = 2$ transition detected around g = 4.5).*

As expected for these Fe(III) complexes, a single weak $\nu_{C\equiv C}$ band is observed in each case in the 1980-1895 cm⁻¹ range (Table 1).[29] The presence of one unpaired electron in 2a-b⁺ is supported by a rhombic ESR signature (Table 3), consistent with ESR signatures previously obtained for related Fe(III) radicals, such as 4[PF₆].[15,29] Similar to observations for 3[PF₆]₂, the ESR signatures of the dinuclear complexes 1a²⁺ and 1b²⁺ were more difficult to detect. Broad featureless signals were observed possibly because of a fast electronic relaxation due to spin-spin interactions in such diradicals.[15]

The ¹H NMR spectra of 1a-b[PF₆]₂ and 2a-b[PF₆] were also recorded and, based on previous work with related derivatives,[32,33] are diagnostic of Fe(III) complexes (See Supporting Information). An assignment for nearly all the observed signals could be proposed for 1a [PF₆]₂ and 2a[PF₆]. The shifts in opposite directions for neighbouring protons on the fluorene group are indicative of opposite spin densities located on the corresponding carbon atoms, consistent with spin delocalization/polarization taking place through the π-manifold.[33,34] For 2a[PF₆], relative to 1a[PF₆], the protons the fluorenyl group are significantly less shifted, consistent with a less marked spin delocalization/polarization on the aromatic ring of the alkynyl ligand that is more remote from the metal center. Nevertheless, these fluorenyl protons experience a significantly larger paramagnetic contribution to their

6

chemical shifts than the corresponding nuclei in **4**[PF$_6$],[32] presumably as a result of the planarity of the fluorenyl group facilitating greater spin delocalization/polarization via the π-manifold compared to that experienced by the non-coplanar 4,4'-biphenyl spacer in **4**[PF$_6$].

Comparison of the chemical shifts observed for the fluorenyl protons in **1a**[PF$_6$]$_2$ and **2a**[PF$_6$] reveals that the protons of **1a**[PF$_6$]$_2$ appear significantly less shifted than those of **2a**[PF$_6$], indicating the possible existence of an antiferromagnetic exchange interaction taking place between the remote Fe(III) endgroups.[33] The existence of intramolecular antiferromagnetic coupling is also suggested by the temperature dependence of the ^{1}H NMR shifts of the fluorenyl protons of **1a**[PF$_6$]$_2$ (Supporting Information); while the chemical shifts can be linearly fitted vs. 1/T (in K^{-1}), a very slight curvature is apparent on the corresponding plots. This is also consistent with the magnetization curve obtained from SQUID measurements on solid samples of **1a**[PF$_6$]$_2$. The data can be fitted to a Curie-Weiss law in the upper temperature range with a thermal variation of the $\chi_M.T$ product almost constant ($\sim$0.82 cm^3 K mol^{-1}) and coinciding with the spin-only value expected for two uncoupled spins S = ½. At temperatures lower than 50 K, $\chi_M.T$ decreases slightly on cooling, a behavior characteristic of an antiferromagnetic interaction between unpaired spins. The latter can be modelled by a Weiss constant of 67 K (ca. 47 cm^{-1}).[35] An averaged antiferromagnetic coupling constant of ca. -12 cm^{-1} (taken over 8 neighbouring Fe(III) centers) corresponding to a singlet-triplet gap of ca. 24 cm^{-1} can be deduced from this constant for **1a**[PF$_6$]$_2$ in the solid state.[36]

Absorption Spectroscopy. The UV-Vis-near-IR absorption spectra of **1a-b**$^{2n+}$ and **2a-b**$^{n+}$ (n = 0, 1) were recorded in dichloromethane (Table 4). For the Fe(II) complexes, the broad absorption band observed at lowest energy (in the range 400-470 nm) results in the orange colour of these compounds (Figure 2). TD-DFT computations indicate that this band largely results from metal-to-ligand charge transfer (MLCT), as previously proposed for the related 4,4'-biphenyl analogues (**3** and **4**) of **1a** and **2a**.[15] Consistent with this involvement of the metal center, this band is not found in the absorption spectra of the corresponding organic alkynes (Table 4) or (trialkylsilyl)alkynes (Supporting Information). The MLCT absorption for **1a** is bathochromically shifted by 46 nm (2530 cm^{-1}) relative to that of **2a**, in line with the slight increase in π-manifold contributing to a decrease in the energy gap between the corresponding MOs (see DFT calculations). Also consistent with the extension of the π-manifold, the spectra of the compounds with extended bridges **1b** and **2b** possess MLCT transitions at lower energy than those of their shorter counterparts **1a** and **2a**. This MLCT absorption is bathochromically shifted for **1b** compared to **2b**, albeit by a smaller energy (ca. 20 nm or 954 cm^{-1}) than between **1a** and **2a**. A similar trend is observed for the next-higher-energy intense absorption band (near 320-370 nm: 27000-31000 cm^{-1}), which, according to calculations, corresponds to a more marked ligand-centred (LC) character of π*←π type on the fluorenyl fragment. This LC transition appears only as a shoulder in the spectra of the smaller complexes **1a** and **2a**. Consistent with this assignment, a transition is present at very similar energies in the spectra of the free ligands **5a'-b'** and **7a'-b'**.
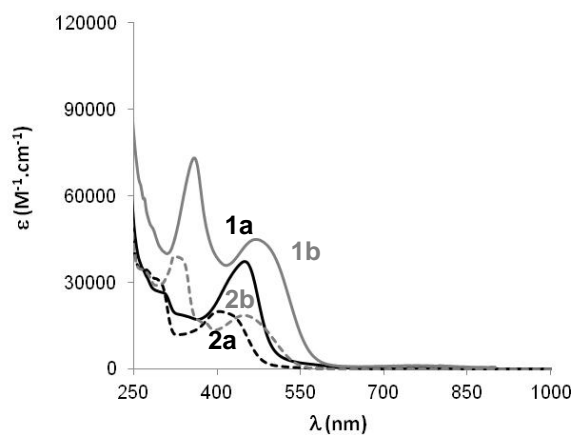

Figure 2. UV-Vis-NIR spectra for **1a-b** and **2a-b** in dichloromethane at 300 K.

Table 4. Absorption and Emission Data for the Fe(II)/Fe(III) Complexes 1a-b^{2n+}, 2a-b^{n+}, 3^{2n+} and 4^{n+} (n = 0, 1) in CH$_2$Cl$_2$.

Cmpd	Absorption: λ_{max}/nm (10^{-3} ε in M^{-1} cm^{-1})	λ_{em} [λ_{ex}]^a /nm	Φ_{lum}	Ref.
1a	264 (sh, 35.5), 304 (sh, 27.5), 450 (37.4)	332 [296]	0.7 %	this work
		$\approx$ 510 [440]	/^{b}	
1a^{2+}	270 (sh, 37.4), 344 (27.7), 496 (8.9), 630 (3.0), 772 (13.7), 820 (sh, 10.7), 1844 (0.4)	333 [294]	1.0 %	this work
2a	278 (sh, 33.4), 296 (sh, 30.0), 404 (20.0)	334 [291]	0.4 %	this work
		507 [403]	0.2 %	
2a$^+$	280 (36.9), 327 (sh, 26.5), 406 (8.3), 466 (4.8), 624 (sh, 1.9), 764 (8.1), 1824 (0.18)	332 [291]	0.8 %	this work
1b	269 (sh, 59.1), 358 (73.2), 468 (45.0)	383 [357]	< 2.9 %^{c}	this work
1b^{2+}	266 (66.0), 374 (101.0), 464 (sh, 14.8), 758 (10.8), 1866 (0.33)	411 [380]	< 1.5 %^{c}	this work
2b	276 (sh, 32.8), 322 (36.9), 380 (14.0), 448 (19.0)	367 [323]^e	0.1 %	this work
2b$^+$	290 (29.3), 346 (48.0), 454 (7.9), 756 (5.6),1860 (0.17)	/	/	this work
3	275 (sh, 42.9), 432 (40.2)	352 [290]	1.3 %	this work and [15]
3^{2+}	278 (sh, 50.4), 334 (sh, 33.0), 464 (sh, 6.8), 623 (3.8), 726 (8.4), 1834 (0.13)	ND^d	ND^d	[15]
4	275 (sh, 34.1), 401 (17.5)	324 [274]	1.4 %	this work and [15]
		428 [388]	0.1%	
4$^+$	280 (sh, 88.2), 370 (sh, 7.2), 440 (sh, 3.0), 613 (2.0), 710 (4.1), 1800 (0.08)	ND^d	ND^d	[15]
5a'	292 (sh, 26.8), 303 (35.8), 317 (sh, 31.0), 329 (48.0)	333, 349 [303]	76 %	this work^e
5b'	237 (39.6), 267 (36.1), 364 (97.3)	390, 411 [364]	78 %	this work
7a'	292 (sh, 34.8), 305 (24.8), 317 (36.5)	319, 331 [292]	58 %	this work
7b'	311 (sh, 32.7), 331 (53.5), 352 (54.6)	380 [331]	58 %	this work
8^f	288 (37.9)	324, 339 [288]	78 %	this work
9^f	273 (30.2)	322 [273]	35 %	this work

^{a} *Emission [excitation] wavelengths.* ^{b} $\Phi_{lum} \approx 0$. ^{c} *Traces of fluorescent organic impurities possibly present.* ^{d} *Not determined.* ^{e} *See also* [38]. ^{f} *See Chart* 2.
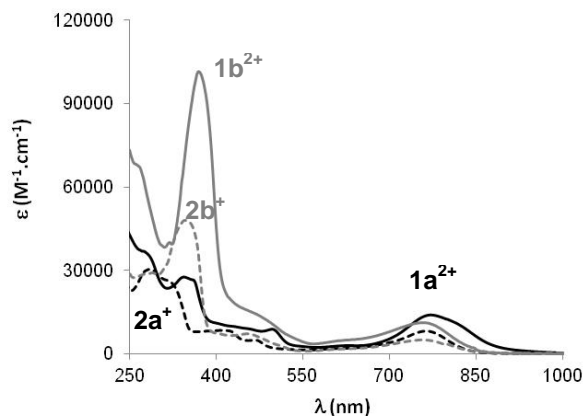

Figure 3. UV-Vis-NIR absorption spectra for **1a-b**[PF$_6$]$_2$ and **2a-b**[PF$_6$] complexes in dichloromethane at 300 K.

The UV-Vis-near-IR spectra of the corresponding Fe(III) complex (di)cations **1a^{2+}**, **1b^{2+}**, **2a$^+$** and **2b$^+$** were also recorded (Table 4 and Figure 3). The dark blue/green colour of these compounds originates from several absorptions in the visible range, with maxima in the 750-800 nm range and most likely corresponding to LMCT bands.[33] These spectra resemble those previously reported for **3**[PF$_6$]$_2$ and **4**[PF$_6$].[15] In contrast to the corresponding Fe(II) complexes, which are silent in the near-IR range, a weak absorption is detected for the Fe(III) complexes near 1850 nm corresponding to a (SOMO-n) to SOMO formally forbidden ligand-field (LF) transition (d$_{Fe}^1$←d$_{Fe}^2$).[15,29] As before, a shift to lower energy is observed for all these absorption bands upon progressing from monocations to dications, the shift being less marked for the extended compounds. Transitions are, in principle, doubly degenerate in the dications when there is a weak or negligible electronic coupling between the corresponding chromophores. As a result, they exhibit a rough doubling in intensity in proceeding to **1b^{2+}** from the mononuclear complex **2b$^+$**. The fluorene-based IL transitions observed at 358 and 380 nm for **1b** and **2b** undergo a bathochromic shift upon oxidation.
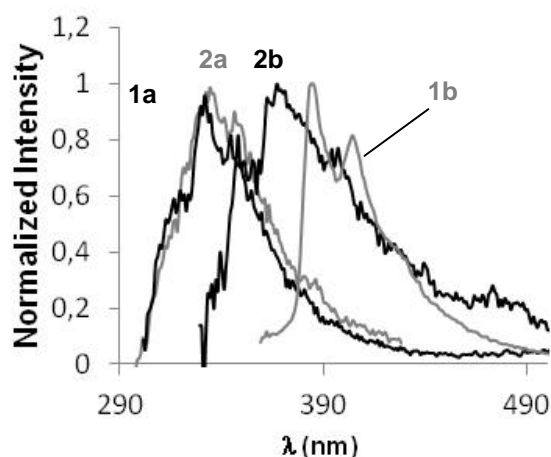
8

Figure 4. UV-Vis emission spectra for **1a-b** and **2a-b** complexes in dichloromethane at 300 K.

Luminescence Studies. Upon excitation in the 285-360 nm range in CH_2Cl_2 solutions at ambient temperatures, all the synthesized fluorenyl-containing Fe(II) and Fe(III) complexes were found to luminesce in a narrow spectral range located in the blue region around 310-380 nm (Figure 4). The fluorescence yields are significantly lower than those of their purely organic fluorenyl alkyne precursors (Supporting information); the yields for **1a-b**$[PF_6]_n$ and **2a-b**$[PF_6]_n$ (n = 0, 1) are all < 2%, whereas yields above 70% were found for alkyne precursors **5a'** and **5b'**, and above 55% for **7a'** and **7b'**.

Several points can be made regarding these organometallic luminophores. First, upon excitation of the Fe(II) complexes in their fluorene-based LC state, some luminescence originates from this state or from a closely lying excited state. This luminescence does not originate from the lowest-lying excited state. Indeed, according to their absorption spectra, at least one other state (MLCT) is present at lower energies (Table 4) and, upon excitation into the MLCT band of compounds such as **1a** or **2a**, only a very weak luminescence of uncertain origin can be detected near 500 nm ($\Phi_{lum} \leq 0.2$ %). A similar behaviour is found for the 4,4'-biphenyl complexes **3** and **4** relative to their organic precursors **8** and **9**. Second, while the organic luminophores **3a-b'** and **5a-b'** exhibit a clear vibronic structure for their fluorene-based LC state,[39] this vibronic structure is far less marked in the emission

spectra of the corresponding complexes. In contrast to the organics, no clear shift in the band envelope of the emission is apparent across the various alkynyl complexes, regardless of the nature of the alkynyl ligands or their oxidation state. Finally, oxidation of the Fe(II) center(s) appear(s) to only marginally affect the luminescence of the compounds **1a-b** and **2a-b**; a broad emission near 330 nm is found in each case, with comparable fluorescence yields within experimental uncertainties. This emission occurs at an energy well above the lowest-lying excited state of the various Fe(III) complexes, but the luminescence of these LMCT states could not be probed due to instrumental limitations.
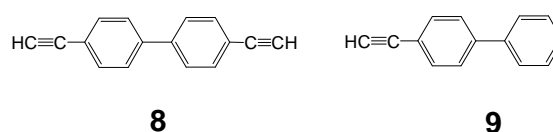

8   **9**

Chart 2. Biphenyl-based Fluorophores in Table 4.

Synthesis and Characterization of the Corresponding Mixed-Valent Fe(II)/Fe(III) Complexes. In order to obtain some information about the properties of the MV complexes **1a**$^+$ and **1b**$^+$, we have attempted to characterize both species *in situ*. The former MV complex was produced by mixing equimolar mixtures of its neutral and dicationic parents in dichloromethane (Scheme 2),[16] while the latter MV complex was generated by reacting the Fe(II) dinuclear precursor **1b** with one equivalent of ferricenium hexafluorophosphate [FcH]$[PF_6]$. According to the K_c values determined from CV, **1a**$[PF_6]$ should be formed in 81 % yield in solution along with 9.5 % of **1a** and 9.5 % of **1a**$[PF_6]_2$, while **1b**$[PF_6]$ should be present in the medium in nearly statistical proportions (50 %) in equilibrium with the starting complex **1b** (25 %) and the corresponding dication **1b**$[PF_6]_2$ (25 %). In the latter case one equivalent of ferrocene is also present in the medium (note that in the spectra obtained, ferrocene can be considered as being almost spectroscopically silent in the 400-2500 nm range[40]).

ESR spectra have been obtained likewise from frozen solutions in CH_2Cl_2/1.2-$C_2H_4Cl_2$ mixtures at 80 K. The signa-

9

tures of both the MV complexes and the dications were observed by ESR (Table 3). Consistent with the strong localization of the unpaired electrons at the metal centers, a rhombic spectrum was obtained in each case, with a slightly lower anisotropy (Δg) than was seen for the corresponding mononuclear Fe(III) model complexes **2a-b**[PF$_6$]. Among pianostool alkynyl complexes, these signatures are typical of a delocalized cationic largely-Fe(III)-centered radical.[29]
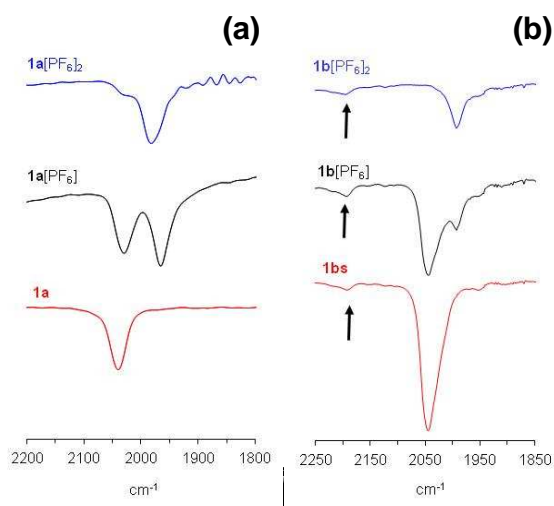

Figure 5. Infrared spectra (KBr window) showing the $\nu_{C \equiv CFe}$ modes of the pure dications, of the comproportionation mixtures and of the pure neutral complexes in dichloromethane for **1a** (a) and **1b** (b). In the latter case, arrows indicate the very weak absorption corresponding to the internal $\nu_{C \equiv C}$ stretch.

The localization of the valency is also evidenced by the infrared spectrum recorded for **1a**[PF$_6$] in solution, which reveals two new strong $\nu_{FeC \equiv C}$ bands overlapping the corresponding modes of **1a** and **1a**[PF$_6$]$_2$ (Figure 5a). For **1b**[PF$_6$], the absorptions apparently overlap with those of **1b** and **1b**[PF$_6$]$_2$ since no new absorptions appear in the comproportionation mixture (Figure 5b). In both cases, these absorptions, typical of Fe(II) and Fe(III) alkynyls, evidence the presence of distinct and localized redox sites in **1a**[PF$_6$] and **1b**[PF$_6$].[41] Consistent with the voltammetric study, these data establish both mixed-valent compounds as either class-I or

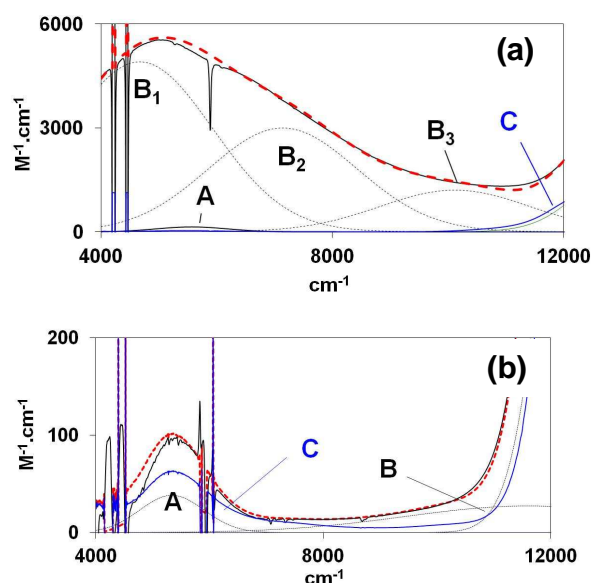class-II MV compounds in the classification of Robin and Day.[42,43]

Figure 6. Near-IR spectra obtained for the comproportionation mixtures of **1a/1a**[PF$_6$]$_2$ (a) and **1b/1b**[PF$_6$]$_2$ (b) in CH$_2$Cl$_2$ and proposed deconvolutions (Sub-bands A-B: see text). The contribution of the corresponding dications are also shown (curves C). The sum of the various contributions (A, B and C) is shown as the red dotted line. A constant background of *ca.* 50 M^{-1}.cm^{-1} has been substracted from spectrum (b) over the complete spectral range to compensate for diffusion effects.

As expected, the reaction mixtures containing the MV complexes **1a**[PF$_6$] and **1b**[PF$_6$] afford absorption spectra resembling the mean spectrum of the those of the parent homovalent complexes in the UV-vis range. However, in the case of **1a**[PF$_6$], clear differences can be seen for the most intense transitions, which appear slightly shifted relative to those detected for pure **1a** and **1a**[PF$_6$]$_2$, in line with the presence of a new species in the medium presenting a lower symmetry than its homovalent parents. Furthermore, in the near-IR range, an intense and *new* absorption is detected at ca. 1970 nm (or 5075 cm^{-1}) that was absent for pure solutions of **1a** and **1a**[PF$_6$]$_2$ (Figure 6a). As mentioned previously, **1a** is silent in this spectral range, whereas **1a**[PF$_6$]$_2$ possesses only

10

a very weak absorption near 1844 nm (5423 cm^{-1}) corresponding to a forbidden ligand field (LF) transition.[15,29] In contrast, for the comproportionation mixture containing **1b**[PF$_6$], the comparably much weaker absorption detected in the near-IR range (Figure 6b) strongly resembles that found for **1b**[PF$_6$]$_2$ near 1866 nm (5459 cm^{-1}).

The broad absorption detected at ca. 5000 cm^{-1} (2000 nm) for **1a**[PF$_6$] was thus considered to be an intervalence charge transfer (IVCT) band diagnostic of this MV complex. However, considering the energy (ν_{max} = 4995 cm^{-1}) of the maximum, the halfwidth [$(\nu_{1/2})_{exp}$ > 6000 cm^{-1}] and also the (non-Gaussian) shape of this band (Figure 6a), it cannot correspond to a single intervalence charge transfer (IVCT) band (see eq. 2) but most likely results from several overlapping bands. As detailed previously,[16] it was deconvoluted into several Gaussian sub-bands (Table 5). The spectral contribution of **1a**[PF$_6$]$_2$ (C) which is present in the medium (9.5 %) has a negligible contribution on the overall band shape. Another contribution (A) stems from a similar LF transition at the Fe(III) site of the MV complex **1a**[PF$_6$]. During the deconvolution process, this weak contribution was simulated with a comparable halfwidth to that of the LF absorption of **1a**[PF$_6$]$_2$ and its energy was kept close to it. As for C, this sub-band (A) should not strongly influence the band shape of the near-IR transition detected for the MV complex. Three additional and much more intense contributions were considered to properly reproduce the observed band shape (B$_1$-B$_3$). Such sub-bands are reminiscent of those proposed in near-IR band deconvolutions of the related organoiron MV derivatives **3**[PF$_6$].[15,44] For pseudo-octahedral MV complexes possessing an unpaired electron in the metal d sub-levels close in energy to the HOMO-1/HOMO-2 levels, and with a sizable metal-metal interaction mediated by the bridging ligand, these sub-bands possibly correspond to the sought-after IVCT and two interconfigurational transitions.[15,45] Thus, the most intense sub-band at lowest energy (B$_1$) is proposed to correspond to the IVCT transition. Consistent with this hypothesis, this sub-band (along with B$_2$ and B$_3$) is hypsochromically shifted when the dichloromethane solvent is replaced by a solvent with a higher dielectric constant such as acetone or acetonitrile (Figure 7). This observation allows us to re-

fine further the classification of the **1a**[PF$_6$] as a class-IIA MV complex.

$$(\nu_{1/2})_{theo} = (2310.\nu_{max})^{1/2} \tag{3}$$

$$H_{FeFe} = (2.06.10^{-2}/d_{FeFe})(\varepsilon_{max}.\nu_{max}.\Delta\nu_{1/2})^{1/2} \tag{4}$$

The sub-bands B$_1$-B$_3$ were considered to have similar half-widths in the deconvolution procedure,[42] with $\nu_{1/2}$ constrained to remain close to the theoretical value predicted by Hush theory (eq 3).[46,47] A reasonable fit can be obtained by this approach (Figure 6a), yielding a sensible reorganization energy for the IVCT ($\lambda \approx$ 4670 cm^{-1}; $\nu_{1/2}$ = 3050 cm^{-1}; ε = 6050 M^{-1}.cm^{-1}) and sensible transition energies for the two interconfigurational processes B$_2$ and B$_3$ (7140 cm^{-1} and 10100 cm^{-1}).[15] A related deconvolution is proposed when acetone is used as solvent.[48]

Table 5. Deconvolution of the Near-IR IVCT Band in Solution and H_{FeFe} derivation for 1a[PF$_6$].

Solvent	Band	ν_{max} in cm^{-1} [a] (ε in M^{-1} cm^{-1}) [b]	$(\nu_{1/2})_{exp}$ (cm^{-1}) [a]	d$_{FeFE}$ (Å) [c]	$(\nu_{1/2})_{theo}$ (cm^{-1}) [d]	H_{FeFe} (cm^{-1}) [a,e]
CH$_2$Cl$_2$	A	5570 (170)	1500	/	3590	/
	B$_1$	4670 (6050)	3050	15.9	3280	380
	B$_2$	7140 (3770)	3050	/	4060	/
	B$_3$	10120 (1490)	3050	/	4830	/
Acetone	A	5570 (180)	1500	/	3660	/
	B$_1$	6790 (6940)	3830	15.9	3960	550
	B$_2$	9190 (3830)	3830	/	4610	/
	B$_3$	12110 (1750)	3830	/	5290	/

[a] Values ± 25 cm^{-1}. [b] Values ± 10 M^{-1}.cm^{-1}. [c] Evaluated from X-ray structure of **1**. [d] Calculated following equation 3. [e] Calculated following equation 4.
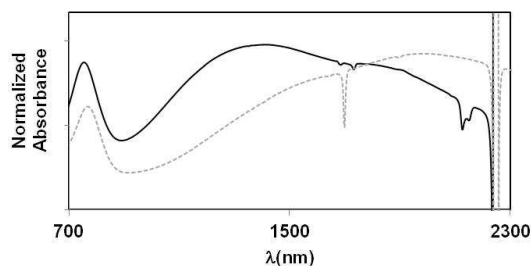

Figure 7. Equimolar Mixture of **1a** and **1a**[PF$_6$]$_2$ in Acetone (Plain Dark Line) and in CH$_2$Cl$_2$ (Dotted Grey Line).

Using the classic Hush equation (eq. 4), a H_{FeFe} value of ca. 380 cm^{-1} was derived for **1a**[PF$_6$] from the energy, intensity and halfwidth of the sub-band C (IVCT). Following a similar procedure, a significantly larger electronic coupling ($H_{FeFe} \approx$ 520 cm^{-1}) was found in acetone, in spite of the lower stability previously evidenced for the MV complex in that solvent. Albeit unexpected, this improvement of the electronic coupling (+45 %) which follows the increase in the polarity of the solvent resembles that (+25 %) previously seen with **3**[PF$_6$].[15,49]

For an extended MV complex such as **1b**[PF$_6$], a less intense and more Gaussian-shaped IVCT transition is expected, due to the unlikely presence of interconfigurational transitions in less coupled MV complexes.[45] Furthermore, its energy should likely be above 6200 cm^{-1}, corresponding to the reorganization energy of the single IVCT process detected for **3**[PF$_6$].[15] In this respect, the weak absorption detected at 5340 cm^{-1} (1873 nm; 160 M^{-1}.cm^{-1}) after substracting the contribution of **1b**[PF$_6$]$_2$ generated in the medium by the comproportionation equilibrium (Scheme 2) certainly corresponds to the LF absorption centred on the Fe(III) site for **1b**[PF$_6$]. However, no other Gaussian absorption band liable to be an intervalence charge transfer (IVCT) band is clearly apparent in the 7000-10000 cm^{-1} spectral range. Actually, the diffusive nature of the concentrated ($> 10^{-3}$ M) samples induces a background absorption which severely complicates the accurate modelization of weak bands. A single broad Gaussian band (B) at $\nu_{max} = 11600$ cm^{-1} (($\nu_{1/2}$)$_{exp} = 5100$ cm^{-1} and $\varepsilon = 45$ M^{-1}.cm^{-1}) would apparently improve the fit (Figure 6b),[51] but such a transition does unlikely correspond to the sought IVCT process, since its energy appears too high for being the reorganization energy of Fe(η^5-C$_5$Me$_5$)(κ^2-dppe) fragments.[15] In addition, its strong overlap with the intense MLCT bands of **1b**[PF$_6$] and **1b**[PF$_6$]$_2$ render actual existence of such a contribution questionable. More complex (multi-band) fitting schemes are thus required to find IVCT band(s) at lower energies, but their interpretation is also more difficult. Anyway, all these fits give IVCT bands corresponding to much weaker electronic couplings

than for **1a**[PF$_6$] and the MV complex **1b**[PF$_6$] can be confidently classified as a weakly coupled class-II (or class-I when no IVCT is considered).

Nonlinear Optical Properties. We next determined the cubic hyperpolarizabilities of several of the molecules by Z-scan, using femtosecond laser pulses at various incident wavelengths between 550 and 1600 nm and as solutions in dichloromethane (as well as THF for **1a-2a**) (Figure 8, Table 6 and Supporting Information). Photochemical changes (color changes of the solution under the laser beam) were seen to occur for **2a** at incident wavelengths less than or equal to 600 nm. This problem was rectified by remaking the solutions and reducing both input power and sample concentration. Other compounds did not exhibit such obvious photochemical effects. **2b$^+$** was found to be unstable over a time span of several days, the dark green **2b$^+$** solution returning to the yellow of **2b** over this period. Samples of **2b$^+$** were therefore remade every day, and appeared to maintain their integrity over the length of a day.

As seen in Table 1, large differences arose between the values of the NLO parameters determined for dichloromethane and THF solutions of the compounds for which both solvents were used. These differences appear too large to be explained by the presence of two-photon solvatochromism,[52] and it is possible that additional mechanisms of nonlinear absorption are operative in dichloromethane solutions in addition to the simple TPA phenomenon, e.g. the absorption by long-lived species formed due to photochemical instability of the compounds although, as mentioned above, photochemical changes were only noted for **2a** (and only at short wavelengths with high incident light power and concentrated solutions). The interpretation of the absolute values of the TPA cross-sections must therefore be cautious, but with this in mind the spectral features and the trends of changes of the parameters between various structures may be analyzed. The cross-sections listed below are those determined for the dichloromethane solutions.

The plots of the real and imaginary parts of γ for **1a** and **1b** show strong dispersion in similar regions: 520-540 nm,

around 620 nm, and 740-760 nm (see Figure 8 for **1a** and Table 1 for **1a** and **1b**). Since the 520-540 nm region coincides with some (weak for **1a** and strong in the case of **1b**) linear absorption, the dominant effects in this region are likely due to excited-state absorption which may appear, depending on the values of the absorption cross-sections of the ground and excited state, as saturable absorption (SA) or reverse saturable absorption (RSA), the former leading to negative contributions to the effective γ_{im} and the latter to positive ones. In contrast, the 620 nm peak of γ_{im} (and thus the peak of the effective TPA cross-section) coincides with twice the λ_{max} value of a (possibly alkyne ligand-centred) π^* $\leftarrow \pi$ transition in **1a**, which is shifted bathochromically with π-bridge extension on proceeding to **1b** (Figure 9) to coincide well with the 720 nm TPA band; the π-bridge lengthening here appears to increase TPA cross-section three-fold. This absorption seems to dominate a small local maximum at 760 nm (2900 GM), which may have similar character to the maximum at 740 nm (2600 GM) seen in the **1a** plot. Oxidation of both species (to generate **1a²⁺** and **1b²⁺**) affords species with linear absorption bands at ca. 760 nm, causing a broad saturable absorption effect at these wavelengths, and resulting in a negative effective TPA cross-section. The redox properties of the molecule can therefore be used to "switch" the sign of the nonlinear absorption in the region of the TPA maxima of the neutral complexes. Oxidation of **1a** also affords a UV-Vis absorption band at 350 nm, a wavelength which corresponds roughly to the TPA maximum seen at 660 nm.

Complexes **2a** and **2a⁺** are (conceptually) fragments of **1a** and **1a²⁺** and exhibit similar effects on the effective TPA cross-sections following oxidation. **2a** has smaller TPA cross-section values and a maximum at the same wavelength, 740 nm, as its bimetallic counterpart. The wavelength of its TPA cross-section peak corresponds closely to twice the wavelength of optical absorption maximum in the UV-Vis spectrum. The linear optical absorption spectrum of **2a⁺** reveals that this oxidized species is less absorptive at ca. 450 nm, with a corresponding absence of SA behaviour at wavelengths in the range 500-560 nm, as observed for **1a⁺**. Simi-

larly, **2b** is a fragment of **1b** and has a similar TPA cross-section spectrum, with peaks at 540, 700, and 760 nm, although maximal values are roughly one fifth of the magnitude of the bimetallic complex. Problems were encountered with highly coloured **2b⁺** in fitting the closed-aperture Z-scan traces in the wavelength range 660-800 nm, accounting for the large errors in the γ_{real} values. The TPA cross-section values for **1b²⁺** are lower than those for its mono-cationic analogue **2b⁺**, probably as a result of the effect of the broader linear absorption bands seen in the 500-660 nm region. Both complex (di)cations exhibit SA in the range 640-800 nm coincident with the longer wavelength TPA maximum of the non-oxidized species.
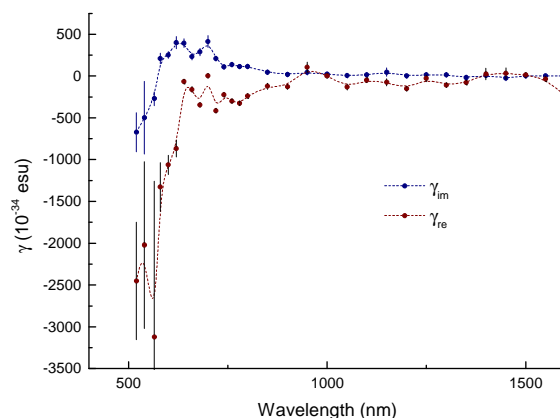

Figure 8. Cubic hyperpolarizabilities determined for **1b** in dichloromethane at 300 K by open and closed-aperture Z-scan measurements.

The biphenyl analogues of the fluorenyl complexes **1a** and **2a** (namely **3** and **4**) both exhibit peaks in the UV/Vis spectra at 580 nm and 700/720 nm (**3**/**4**). Again, the bimetallic complex (**3**) has larger nonlinear absorption cross-sections than its monometallic counterpart, as observed with the previous compounds. TPA maxima appear at shorter wavelengths than for the fluorenyl-containing analogues. The dioxidized species, **3[PF₆]₂**, also exhibits blue-shifted TPA cross-section peaks/troughs, with a maximum at 540 nm (660 nm for **1a²⁺**) and a minimum around 700 nm (760 nm for **1a²⁺**).

13

Table 6. Nonlinear Optical Data at Wavelengths of Apparent TPA Extrema in CH_2Cl_2 (unless otherwise indicated).

	λ (nm)	γ_{re} (10^{-34} esu)	γ_{im} (10^{-34} esu)	$|\gamma|$ (10^{-34} esu)	σ_2 (GM)
1a[a,b]	740	-60 ± 10	16 ± 5	62 ± 10	390 ± 25
1a[a]	740	-59 ± 37	26 ± 6	62 ± 37	680 ± 120
1a	540	-700 ± 63	110 ± 13	710 ± 64	5800 ± 810
	620	-78 ± 16	110 ± 13	130 ± 20	4300 ± 520
	740	-110 ± 10	81 ± 12	140 ± 15	2300 ± 310
1a[2+]	520	-1500 ± 300	-33 ± 10	1500 ± 300	-1900 ± 670
	660	-530 ± 26	76 ± 12	540 ± 29	2700 ± 440
	760	-500 ± 24	91 ± 16	510 ± 29	-2500 ± 430
	1000	28 ± 40	29 ± 12	40 ± 42	450 ± 180
1b	560	-2400 ± 676	-210 ± 65	2400 ± 680	-10000 ± 3200
	620	-680 ± 78	310 ± 56	750 ± 96	13000 ± 2300
	720	-320 ± 16	160 ± 22	360 ± 27	4900 ± 650
	760	-260 ± 10	110 ± 17	280 ± 20	2900 ± 480
	950	83 ± 40	34 ± 10	90 ± 41	590 ± 180
1b[2+]	540	-960 ± 37	30 ± 5	960 ± 37	-1600 ± 260
	700	-240 ± 51	-36 ± 6	240 ± 51	-1200 ± 220
	850	-73 ± 40	25 ± 5	77 ± 40	530 ± 110
	1000	75 ± 50	-20 ± 8	78 ± 51	310 ± 120
2a[a,b]	740	-49 ± 15	3 ± 10	49 ± 18	95 ± 10
2a[a]	740	-25 ± 15	14 ± 2	28 ± 15	330 ± 50
2a	620	-170 ± 15	64 ± 11	180 ± 19	2600 ± 430
	740	-160 ± 17	84 ± 16	180 ± 25	2400 ± 470
2a[+]	540	-2800 ± 50	21 ± 6	2800 ± 50	1100 ± 290
	640	-48 ± 9	18 ± 3	51 ± 9	700 ± 120
	760	-99 ± 10	-11 ± 2	100 ± 10	-300 ± 45
	950	-3 ± 1	16 ± 5	16 ± 6	280 ± 92
2b	540	-520 ± 20	34 ± 5	520 ± 20	-1800 ± 270
	580	-260 ± 20	36 ± 6	270 ± 20	1600 ± 270
	700	-85 ± 10	31 ± 5	90 ± 11	1700 ± 33
	760	-87 ± 9	14 ± 2	88 ± 9	370 ± 60
2b[+]	600	-1400 ± 17	140 ± 16	1400 ± 24	6000 ± 2000
	760	-1200 ± 32	-250 ± 76	1200 ± 330	-6700 ± 2100
	900	5 ± 2	33 ± 6	33 ± 6	620 ± 110
3	580	-520 ± 40	210 ± 27	560 ± 50	9900 ± 1200
	700	-140 ± 15	130 ± 25	200 ± 27	4200 ± 750
	760	-150 ± 7	39 ± 8	155 ± 10	1000 ± 170
3[2+]	540	-430 ± 25	30 ± 6	430 ± 24	1600 ± 340
	700	-420 ± 47	-28 ± 6	430 ± 48	-920 ± 200
	950	-22 ± 24	30 ± 8	37 ± 25	520 ± 140
4	580	-200 ± 50	27 ± 8	200 ± 50	730 ± 200
	720	-250 ± 60	23 ± 7	260 ± 60	670 ± 230

[a] Determined in THF. [b] Data obtained at Wroclaw University of Technology. All other date were obtained at the Australian National University.
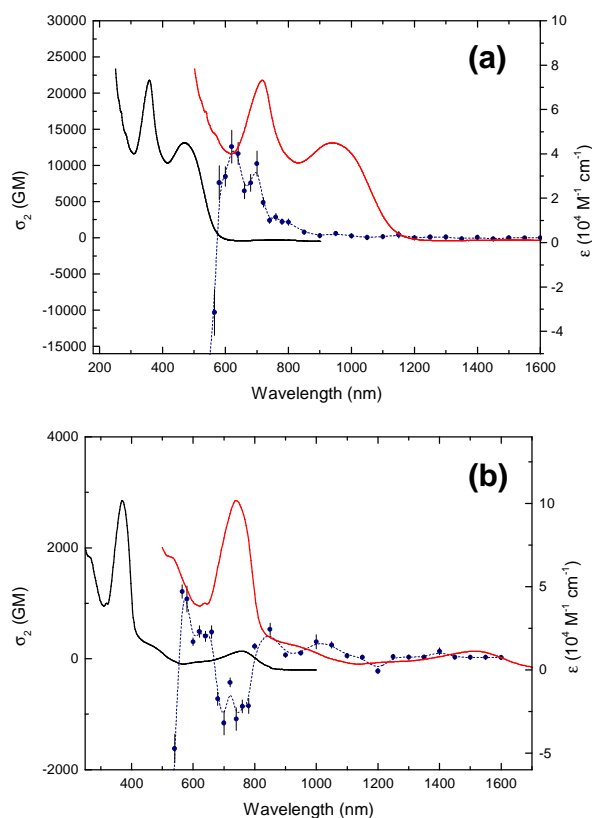
Figure 9. Apparent two-photon absorption cross-sections (in Göppert-Mayer units) for **1b** (a) and **1b^{2+}** (b) in dichloromethane at 300 K by open-aperture Z-scan measurements. The TPA spectral data are overlaid by the one-photon absorption spectrum (black) and the one-photon absorption spectrum plotted at 2λ (red).

Furthermore, comparing the third-order NLO data obtained for **1a/1a^{2+}** and **3a/3a^{2+}** or for **2a** and **4** at the wavelength of the first MLCT band, the γ values are nearly the same within the binuclear and mononuclear sets of complexes, however, the effective TPA cross-sections found for the fluorenyl-containing complexes are always significantly larger in magnitude than those found for the corresponding biphenyl ones. The incorporation of fluorenyl units therefore red-shifts and increases the magnitude of two-photon absorption effects in these molecules.In general, several property-structure relationships can be derived by this study, while being mindful of the error margins and the uncertainties concerning the solvent effects on the effective TPA cross-

sections. Firstly, oxidation/reduction of these compounds can be used to switch between SA and TPA behavior at certain wavelengths. Secondly, compounds with two metal centers and π-bridge extension have larger TPA cross-sections, and at red-shifted wavelengths. Thirdly, replacing biphenyl by fluorenyl also shifts the TPA maxima bathochromically, although values at the short wavelengths are diminished in magnitude.

DFT Calculations. Calculations on C_{2v}-symmetric **1a-Me, 1b-Me** and on C_s-symmetric models **2a-Me** and **2b-Me**, which differ from **1a-b** and **2a-b** by replacement of the dppe ligands by dmpm (bis(dimethylphosphino)methane) and the *n*-butyl groups on the fluorenyl unit by methyl groups), have been performed. After structural optimization (Supporting Information), the calculations reveal that the character of the frontier molecular orbitals (FMO) of the shorter (**1a-Me** and **2a-Me**) and longer (**1b-Me** and **2b-Me**) complexes are in general very similar, a reduction in the HOMO-LUMO gap being seen in each case upon proceeding from the mononuclear to the dinuclear complex (Figures 10 and 11). For all complexes, the three highest-energy occupied orbitals (HOMO, HOMO-1 and HOMO-2) are strongly localized on the organoiron endgroups and nearby alkynyl fragments, while the LUMO in general possesses a strong fluorenyl character. Thus, the assignment of the first oxidation step as mostly metal-localized is appropriate. Close comparison of the dinuclear and mononuclear complexes reveals that extending the alkynyl ligand results in a decrease of the HOMO-LUMO gap, as expected from the extended conjugation within the extended alkynyl ligands. A noticeable feature here is the appearance of two new alkynyl ligand-centred vacant MOs between the LUMO and the metal-based LUMO+1 upon proceeding from **1a-Me** to **1b-Me** (and from **2a-Me** to **2b-Me**), which indicates a slight change in the empty FMOs for the longer derivatives.

TD-DFT calculations were performed on the Fe(II) complexes in order to gain some insight into the nature of the allowed low-energy transitions in the visible range (Table 7).
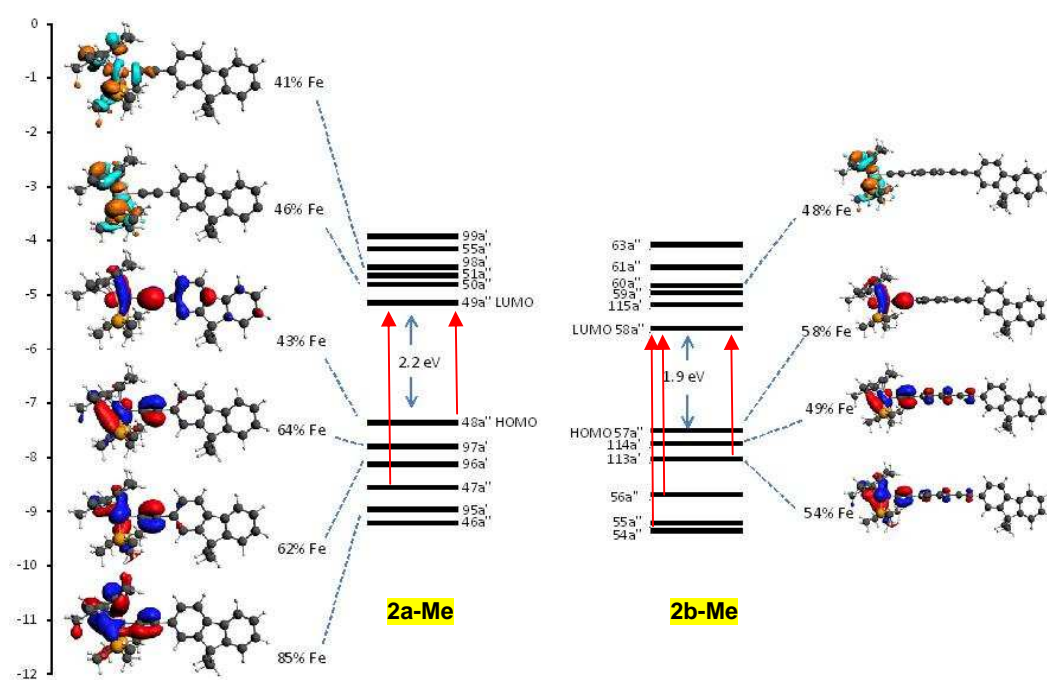
15

Figure 10. Frontier molecular orbitals for **2a-Me** and **2b-Me** illustrating the first allowed calculated transitions (red arrows). The metal-centered MOs are also shown.
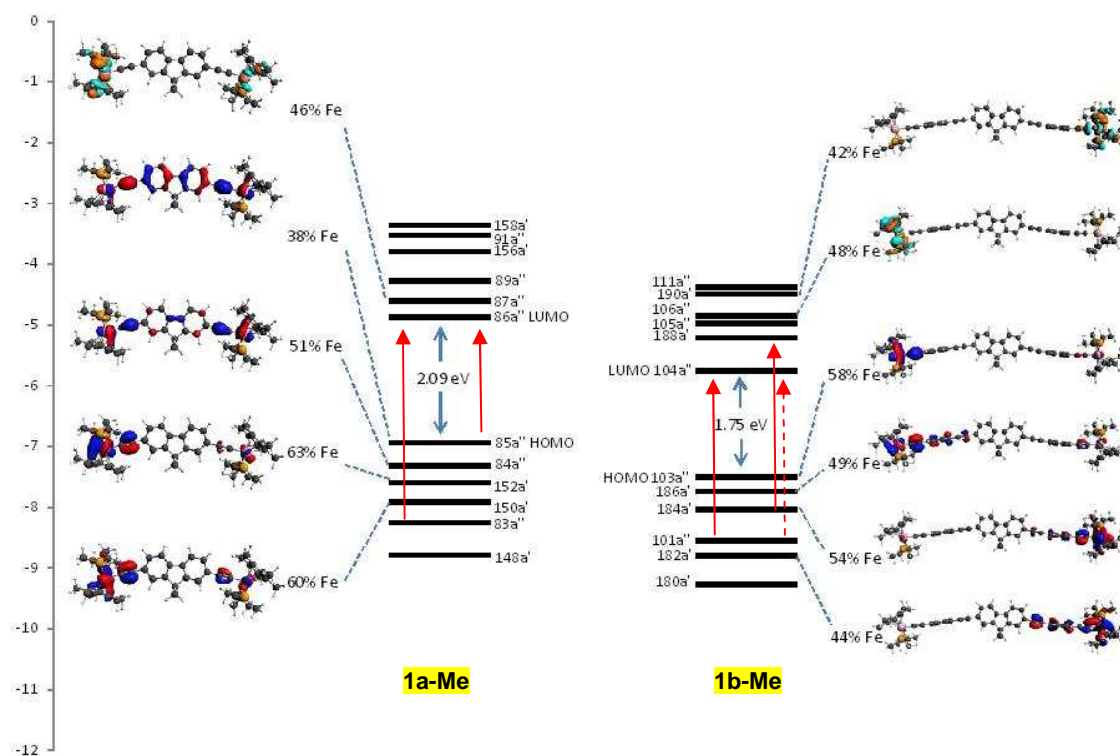

Figure 11. Frontier molecular orbitals for **1a-Me** and **1b-Me** illustrating the first allowed calculated transitions (red arrows). The metal-centered MOs are also shown.

Table 7. Observed and Calculated Optical Transitions for 1a-Me, 1b-Me, 2a-Me and 2b-Me.

Cmpd	$\nu_{max}{}^{a}\,[\varepsilon]^{b}$ (Exp)	$\nu_{max}{}^{a}\,[f]^{c}$ (Calc)	Composition (Weight %)	Major Assignment
2a-Me	24752 [0.20]	20717 [0.12]	48a'' → 49a'' (92%)	Fe_{dxz} (37%) + Fe_{dyz} (6%) + πC_2 + $\pi_{C2Ph} \to \pi^*_{PhFluo}$
	33783 [0.30]	30916 [0.11]	47a'' → 49a'' (53%)	Fe_{dxz} (17%) + Fe_{dyz} (7%) + $\pi_{PhFluo} \to \pi^*_{PhFluo}$
2b-Me	22321 [0.19]	25492 [0.22]	113a' → 115a' (53%)	Fe_{dz2} (50%) + $\pi_{C2} \to \pi^*_{C2Ph}$
	26316 [0.14]	29910 [0.16]	56a'' → 58a'' (48%)	π_{C2} + $\pi_{PhFluo} \to \pi^*_{C2}$ + π^*_{PhFluo}
	31056 [0.37]	30113 [0.09]	54a'' → 58a'' (62%)	Fe_{dxz} (13%) + Fe_{dyz} (11%) + π_{C2} + $\pi_{Cp*} \to \pi^*_{C2}$ + π^*_{PhFluo}
	36232 [0.33]	35254 [0.07]	111a' → 115a' (48%)	π_{Cp*} + π_{C2} + $\pi_{Ph} \to \pi^*_{C2Ph}$
1a-Me	22222 [0.37]	19734 [0.26]	85a'' → 86a'' (69%)	Fe_{dxz} (18% + 15%) + π_{C2} + $\pi_{PhFluo} \to \pi^*_{C2}$ + π^*_{PhFluo}
	32895 [0.27]	30131 [0.12]	83a'' → 86a'' (48%)	Fe_{dxz} (17% + 11%) + $\pi_{PhFluo} \to \pi^*_{C2}$ + π^*_{PhFluo}
1b-Me	21367 [0.45]	24917 [0.44]	101a'' → 104a'' (20%) 184a' → 188a' (15%)	π_{C2} + $\pi_{PhFluo} \to \pi^*_{C2}$ + π^*_{PhFluo} Fe_{dz2}+ $\pi_{C2} \to \pi^*_{C2Ph}$
	27933 [0.73]	27662 [0.08]	101a'' → 104a'' (66%)	π_{C2} + $\pi_{PhFluo} \to \pi^*_{C2}$ + π^*_{PhFluo}
	37175 [0.59]	35252 [0.10]	180a' → 189a' (18%) 180a' → 188a' (16%) 181a' → 188a' (15%)	Fe_{dxy} + π_{C2Ph} + $\pi_{Cp*} \to \pi^*_{C2Ph}$ Fe_{dxy}+ π_{C2Ph} + $\pi_{Cp*} \to \pi^*_{C2Ph}$ Fe_{dxy} + Fe_{dx2-y2} + π_{C2Ph} + $\pi_{Cp*} \to \pi^*_{C2Ph}$

[a] Calculated (for **1a-Me**, **1b-Me**, **2a-Me** and **2b-Me**) and observed (for **1a-b** and **2a-b**) ν_{max} in cm^{-1}. [b] Extinction coefficient in $10^5\ M^{-1}\ cm^{-1}$. [c] Calculated oscillator strength.
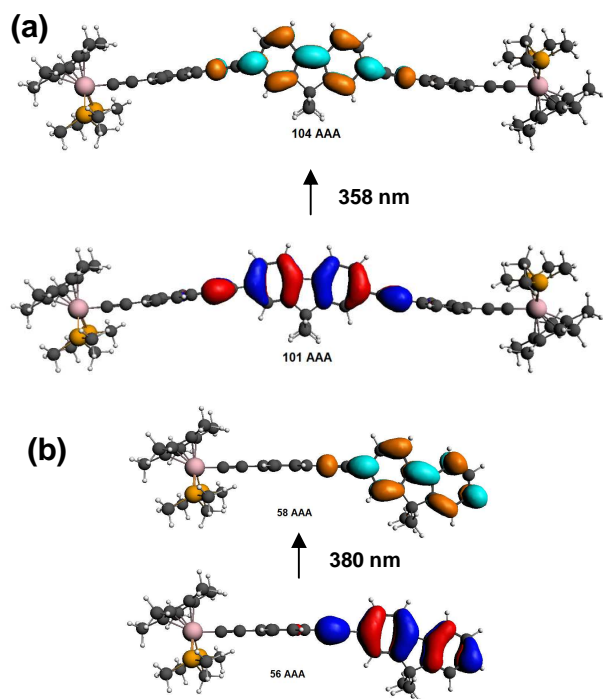
Figure 12. Plots of the frontier molecular orbitals for **1b-Me** (a) and **2b-Me** (b) primarily involved in the second allowed transitions. Contour values are ± 0.03 (e/bohr^3)$^{1/2}$.

Two strongly allowed transitions are found for the mononuclear complex **2a-Me**, the lowest energy corresponding to the LUMO ← HOMO transition with a dominant MLCT character ($\pi^*_{Fluorene} \leftarrow d_{Fe}$), and the second-lowest-energy to a LUMO ← HOMO-5 transition with a strong LC character ($\pi^*_{Fluorene} \leftarrow d_{Fe}$) predominantly centered on the fluorene fragment. For **2b-Me**, the same picture holds except that the MLCT transition at lowest energy changes slightly and corresponds now to a charge transfer towards the phenyl rings of the organic bridge rather than toward the fluorenyl fragment ($\pi^*_{Ph} \leftarrow d_{Fe}$) while a second allowed transition toward the fluorenyl fragment takes place at higher energy (Figure 12). However, contrary to experimental observations, the first transition is now computed to experience a blue shift relative to that in **2a-Me**. For the dinuclear complexes **1a-Me** and **1b-Me**, related allowed transitions are found with the same dominant character but at a slightly lower energy than in the corresponding mononuclear complexes, in line with the slight bathochromic shift experimentally observed.

DISCUSSION

Intramolecular Electron-Transfer in the Mixed-Valent Organoiron Complexes 1a[PF$_6$] and 1b[PF$_6$]. As previously shown,[16] **1a**[PF$_6$] is a better molecular wire than **3**[PF$_6$],[15] as evidenced by the larger electronic coupling deduced for the former complex from the intervalence charge-transfer band ($H_{FeFe} = 380$ cm^{-1} vs. $H_{FeFe} = 145$ cm^{-1}, respectively). This can be attributed to the planarity of the central 2,9-fluorenyl group in **1a**[PF$_6$] compared to the non-planar 4.4'-biphenyl unit in **3**[PF$_6$]. The structural planarity of the central spacer certainly results in a slightly more electron-releasing character for the coplanar 2-fluorenyl core compared to the 4-biphenyl core, as evidenced by the redox potentials of the corresponding mononuclear complexes **2a** and **7** (Table 2; the metal-centered oxidation is slightly easier in **2a** than in **4**). Furthermore, the rigid and planar structure of the former likely promotes enhanced electronic interactions between the redox-active endgroups in **1a**[PF$_6$] relative to those in **3**[PF$_6$]. This feature, further supported by the larger spin polarization of the aryl group evidenced by ^{1}H NMR for **2a**[PF$_6$] relative to **4**[PF$_6$], is probably at the origin of the larger electronic coupling and of the larger redox splitting ($\Delta E° = 110$ vs. 60 mV) in **1a**[PF$_6$]. As a result, this MV complex is class-IIB,[42,43,47] whereas **3**[PF$_6$] certainly belongs to the class-IIA.[15]

Thus, in spite of the loss of axial symmetry of the 2,7-fluorene spacer which might have been at the origin of detrimental quantum interferences compared to the 4,4'-biphenyl spacer,[53] we have established that the 2,7-fluorenyl spacer significantly improves the electronic communication between the [(η^5-C$_5$Me$_5$)(κ^2-dppe)FeC≡C]$^{n+}$ (n = 0, 1) redox active endgroups in the corresponding MV complex. In dichloromethane, when compared to **3**[PF$_6$], this translates to a large improvement in stability constant (K_c) of **1a**[PF$_6$] in the comproportionation equilibrium (Scheme 2), and in a smaller improvement (2.6 fold) in the electronic coupling between the redox endgroups, leading to the observation of interconfigurational IVCT bands, as previously observed

with the class-IIB MV complex **10**[PF$_6$]$_2$ (Chart 3).[15] From the H_{FeFe} value(s), the end-to-end electron transfer is now clearly adiabatic for **1a**[PF$_6$] ($H_{FeFe} \geq 200$ cm^{-1}),[54] and is much faster than in the class-IIA MV analogue **3**[PF$_6$]. Along the same lines, an enlarged intramolecular antiferro-magnetic interaction between the unpaired spins is seen by SQUID and ^{1}H NMR measurements for **1a**[PF$_6$]$_2$. The for-mer has increased by an order of magnitude relative to that previously found for the dication **3**[PF$_6$]$_2$ (- $J_{FeFe} \leq 1$ cm^{-1}),[33] which is also likely to be attributable to the enhanced elec-tronic communication mediated by the 2,7-fluorenyl spacer.

However, further symmetric extension of the unsaturated spacer, in progressing from **1a**[PF$_6$] to **1b**[PF$_6$], does not preserve a large electronic coupling between the terminal organoiron endgroups, as revealed by the difficulty in identi-fying a sensible IVCT transition for this MV complex in the near-IR range.[55] The strongly decreased electronic interac-tion **1b**[PF$_6$] is confirmed by CV, for which the absence of any sizeable extra stability for the MV complex is patent, resulting in a K_c value close to the statistical limit. **1b** can therefore be regarded as a class-I or borderline class-I/class-IIA MV complex.[42,43]
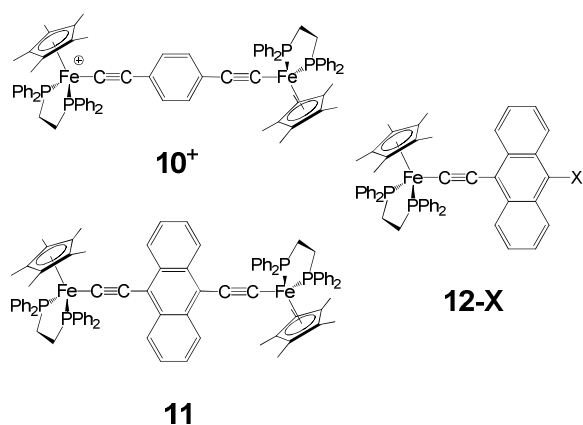

10$^+$

12-X

11

Chart 3. Selected Organoiron Complexes.

Fluorescence Trapping with Organoiron Chromophores 1a-b and 2a-b. When [Fe(η^5-C$_5$Me$_5$)(κ^2-dppe)]$^{n+}$ (n = 0, 1) endgroups are appended to (2-ethynyl)fluorenyl or 2,9-bis(ethynyl)fluorenyl ligands, which are otherwise powerful organic luminophores, an efficient quenching of the lumines-cence takes place, regardless of the oxidation state of the organoiron endgroups. The weak luminescence detected for either the Fe(II) or Fe(III) complexes near 330 nm does not originate from their lowest-lying excited state, but possibly from a fluorene-based LC state. Such an emission from a higher excited state localized on the organic chromophore has previously been observed in related complexes.[56,57] The lack of sensitivity of this emission toward structural modifi-cations is consistent with the strong localization of this ex-cited state on the fluorenyl fragment, as suggested by DFT calculations.

For the Fe(II) complexes, we have experimentally estab-lished that the lowest (MLCT) excited states are not lumi-nescent. A reductive trapping of the fluorene-based excited state could thus be at the origin of the luminescence quench-ing process,[58] as previously proposed with closely related compounds.[57,59] However, the comparable efficiency of the fluorescence-quenching process subsequent to oxidation suggests that another mechanism must also be operative for these complexes in their Fe(III) state. While an oxidative trapping process or an energy transfer process toward the low lying MLCT state might be proposed,[57] further studies are needed to shed sufficient light on the actual trapping mechanism operative in these organometallic chromophores. Overall, these results are reminiscent of observations made on 9-ethynylanthracenyl and Fe(II/III) complexes such as **11** or **12-X** (X = H, Br, CN; Chart 3).[57] In contrast to related dyads incorporating [Fe(η^5-C$_5$Me$_5$)(κ^2-dppe)C≡C]$^{n+}$ end-groups, the luminescence of the chromophore appended to the alkynyl bridge in **1a-b** and **2a-b** cannot be significantly switched by changing the oxidation state of the organoiron moiety.[59]

Redox-dependant Cubic NLO Properties of the Organoi-ron Chromophores 1a-b, 2a-b, 3 and 4. As is usually ob-served for such electron-rich d^6-metal alkynyl complexes, the real part of the cubic molecular polarizability dominates the modulus of χ.[20] It is overall negative in the visible range with the sign invariant between the different oxidation states of a

given compound.[60] In contrast, the imaginary part (χ_{im}) of the present complexes can be positive or negative in sign, depending on the wavelength and on the oxidation state probed; these compounds can therefore give rise to markedly different nonlinear absorption responses at specific wavelengths as a function of oxidation state. If thermal effects are minimized, as is the case for low repetition rate femtosecond laser measurements, the value of the imaginary part of γ reflects the underlying electronic phenomena induced by nonlinear absorption processes such as SA, RSA or TPA.[61] These data can therefore be used to derive their magnitude. Negative χ_{im} values correspond to SA processes, while positive values may correspond to RSA or TPA processes. In general, positive χ_{im} values seen in the spectral regions with no one-photon absorption should reflect underlying TPA phenomena while RSA may be present where one-photon absorption becomes important; "effective" TPA values can be quoted in both cases.

For the Fe(II) mononuclear complexes, the energy of the excited state populated by the apparent TPA process at lowest energy does not coincide with that of the lowest lying MLCT state but is blue-shifted. Calculations indicate that it corresponds to an excited state with a larger organic/$\pi* \leftarrow \pi$ character. The energy of this TPA peak for **2b** matches that of the fluorene-based LC state. The same trend can also be observed for the corresponding dinuclear complexes, but given the exclusion rule between one-photon and two-photon absorption processes in centrosymmetric chromophores, no match between these states is expected for the dinuclear complexes.[62] Similar to many purely organic fluorenes, the Fe(II) complexes **1a-b** exhibit significant TPA in the 700-800 nm range. The organoiron complexes appear to exhibit most often (much) larger cross-sections than organic chromophores of comparable length, even in THF where no underlying photochemistry can be suspected to contribute. For instance, TPA cross-sections of 1200 GM at 705 nm and 130 GM at 600 nm (Chart 4) have been reported for **13** and **14**, respectively.[2,12] Likewise to what has been previously stated for the organoiron complexes **1a**, **2a**, **3** and **4**, the biphenyl analogue **15** also has a lower TPA cross-section

(380 GM at 735 nm) (Chart 4), and a linear absorption maximum at shorter wavelengths,[8] features likely resulting from non-planarity of this chromophore. Among planar chromophores, dinuclear chromophores **1a-b**, with a pseudo-quadrupolar structure, are better two-photon absorbers than their purely "dipolar" counterparts **2a-b**, consistent with common observations.[63] Sizeable positive values of the imaginary part of the cubic molecular polarisability (χ_{im}) are seen for these compounds in a spectral range where they are not absorbing.

In the corresponding Fe(III) complexes, a strong LMCT peak is usually present at the red edge of the visible range (Table 4).[29] Absorption of incident light followed by a SA process takes place, resulting in a negative "apparent" TPA value and a negative χ_{im} value in this spectral region. Similar to observations with related homometallic,[27,60,64] or heterometallic[65] alkynyl complexes of d^6-metal centers, oxidation provides a simple means to dramatically alter the cubic absorptive LO and NLO behaviour of these complexes in the 700-800 nm spectral range, the effect being largest with the extended compound **1b**. This constitutes the second example where a strong redox-switching is evidenced in this spectral range for homometallic Fe(II) complexes.[27] In the present case, extending the carbon-rich spacer has a positive effect on this particular property.
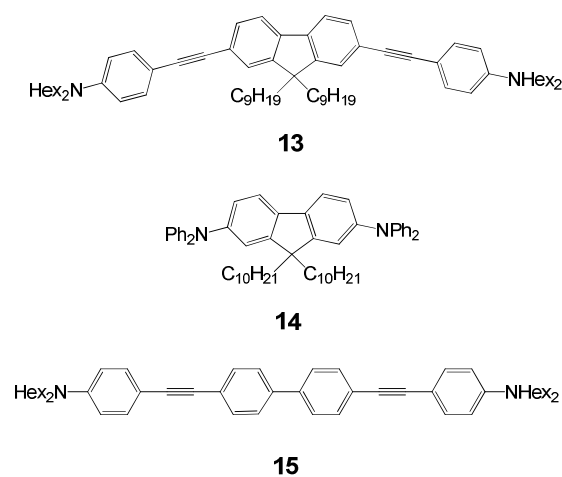

Chart 4. Example of Organic Biphotonic Absorbers.

A beneficial effect of these redox-active organoiron derivatives over the organoruthenium ones is that the open-shell complexes are kinetically more stable. Thus, the Fe(III) derivatives can be chemically isolated which is virtually impossible with their Ru(III) counterparts;[66] the Fe(III) complex cations can be electrochemically generated from their Fe(II) precursors at a more moderate potential by coulometry in the OTTLE cell.

CONCLUSION

We have reported herein the synthesis of a series of new mono- and dinuclear organoiron fluorenylalkynyl complexes in their Fe(II)/Fe(III) oxidation states and investigated their redox and optical properties.

As assessed from studies of the intermolecular electron-transfer properties of the dinuclear complexes in their MV state, the shorter complex **1a**[PF$_6$] was shown to be a much more efficient molecular wire than the known 4,4'-biphenyl analogue (**3**[PF$_6$]). This improvement can be traced to the planarity of the central aromatic unit, which is more suited to convey electronic interactions between the terminal metal centers through the π-manifold of the carbon-rich spacer. Similar investigations on **1b**[PF$_6$] revealed that symmetric extension of the central bridge by two 4-phenylethynyl units does not preserve a sufficiently strong metal-metal electronic coupling to allow unambiguous detection of the IVCT transition. Accordingly, no extra stability is seen for the extended MV complex.

In studies of the optical properties of these redox-active organometallic chromophores, we have observed a strong quenching of their fluorene-based luminescence, which occurs regardless of the oxidation state of the organometallic termini, negating their potential use as redox-switchable luminophores. However, Z-scan measurements over a large wavelength range (400-1600 nm) have revealed sizeable cubic molecular polarizabilities in the visible region for these species. The two-photon absorption properties of the fluorene-containing ligands are preserved in these compounds, which exhibit significantly larger apparent TPA cross-sections in CH$_2$Cl$_2$ than purely organic derivatives of similar size. This enhancement might be attributed to the presence of the electron-releasing organometallic capping groups featuring polarizable metal centers. The dinuclear compounds are more active than the mononuclear complexes, and **1b** is much more active than **1a**, presumably due to its more extended π-manifold. The planarity of the central 2,7-fluorene unit has certainly also a beneficial effect on the TPA cross-sections at the wavelength of the first transition with a large fluorene character, as revealed by the comparison with the 4,4'-biphenyl analogues **3** and **4**.

We have reported the second example of homobimetallic organoiron complexes functioning as redox-switchable nonlinear electrochromes, and thereby revealed their potential for controlling the cubic NLO response. Again, this remarkable behaviour results from the combined effect of a strong two-photon absorption for the Fe(II) complexes, and from SA occurring in the same spectral range for the corresponding Fe(III) complexes. The latter is triggered by the appearance of a strong (LMCT) absorption upon oxidation. Furthermore, compared to the known ruthenium-based analogues operative in the same wavelength range, these new derivatives afford the advantage of being redox-switchable at lower applied potentials in the OTTLE cell, and exhibiting increased kinetic stability in their oxidized state.

EXPERIMENTAL SECTION

General Data. All manipulations were carried out under an atmosphere of inert argon. Solvents and reagents were used as follows: MeOH, distilled from MgOMe; THF, Et$_2$O and *n*-pentane, distilled from Na/benzophenone; CH$_2$Cl$_2$, distilled from CaH$_2$ and purged with Ar, opened/stored under Ar. High field NMR spectra experiments were performed on a multinuclear Bruker 500 MHz, 300 MHz or 200 MHz instrument. Chemical shifts are given in parts per million (ppm) relative to tetramethylsilane (TMS) for ^{1}H and ^{13}C NMR spectra and external H$_3$PO$_4$ for ^{31}P NMR spectra. Experimental details regarding measurements on paramagnetic Fe(III) complexes can be found in previous contributions.[32,33]

Transmittance-FTIR spectra were recorded using a Bruker IFS28 spectrometer (400-4000 cm^{-1}). Raman spectra of the solid samples were obtained by diffuse scattering on the same apparatus and recorded in the 100-3300 cm^{-1} range (Stokes emission) with a laser excitation source at 1064 nm (25 mW) and a quartz separator with a FRA 106 detector. UV-Visible spectra were recorded using a Cary 5000 apparatus in the 200-2500 nm range. Fluorescence spectra were recorded using a FLS 920 Edinburgh Instrument spectrophotometer. MS analyses were performed at the "Centre Regional de Mesures Physiques de l'Ouest" (CRMPO, University of Rennes) on a high resolution MS/MS ZABSpec TOF Micromass Spectrometer. Elemental analyses were performed at CRMPO. The single-crystal X-ray diffraction studies were carried out at the "Centre de Diffractométrie X" (UMR CNRS 6226, University of Rennes).

Unless specified, all reagents were of commercial grade. The synthesis of the organic alkyne precursors **5a'-b'**, and **7a'-b'** is given as Supporting Information. Compounds **5a'** and **7a'** were also recently synthesized via other synthetic approaches.[67] 4-Ethynylbiphenyl (**8**), 4,4'-diethynylbiphenyl (**9**) and Fe(η^5-C$_5$Me$_5$)(κ^2-dppe)Cl (**6**) were prepared according to published procedures.[15,68]

Synthesis of Fe(η^5-C$_5$Me$_5$)(κ^2-dppe)C≡C(2,7-C$_{13}$H$_6$/Bu$_2$)C≡C-Fe(η^5-C$_5$Me$_5$)(κ^2-dppe) (1a). Fe(η^5-C$_5$Me$_5$)(κ^2-dppe)Cl (**6**, 842 mg, 1.35 mmol, 2.0 eq), 2,7-diethynyl-9,9-dibutyl-9H-fluorene (**5a'**, 220 mg, 0.67 mmol, 1.0 eq) and KPF$_6$ (273 mg, 1.4 mmol, 2.2 eq) were dissolved in MeOH (30 mL) in a Schlenk tube. The solution was stirred and heated to 35 °C for 12 h. The brown suspension was allowed to settle and was filtered. The solid was washed with deoxygenated MeOH (2 × 10 mL) at 0 °C and extracted with CH$_2$Cl$_2$. The solvent was removed and the solid was dried under vacuum to afford a brown solid which was characterized by NMR as the bis-vinylidene complex [Fe(η^5-C$_5$Me$_5$)(κ^2-dppe)C=CH(2,7-C$_{13}$H$_6$/Bu$_2$)HC=CFe(η^5-C$_5$Me$_5$)(κ^2-dppe)](PF$_6$)$_2$ (**1a-v**[PF$_6$]$_2$; 834 mg, 61 %). IR (KBr, cm^{-1}): ν = 1623 (s, Fe=C=C); 1600 (s, C=C$_{Flu}$). ^{31}P{^{1}H} NMR (81 MHz, CDCl$_3$): δ = 89.1 (s, P_{dppe}), -143.1

(hept, $^1J_{P,F}$ = 713 Hz, PF$_6^-$). ^{1}H NMR (200 MHz, CDCl$_3$): δ = 7.60-7.10 (m, 42H, H_{Flu} and $H_{Ph/dppe}$), 6.48 (s, 2H, H_{Flu}), 6.23 (d, 2H, $^3J_{H,H}$ = 8 Hz, H_{Flu}), 5.26 (m, 2H, =CH), 3.10 (m, 4H, CH$_{2/dppe}$), 2.51 (m, 4H, CH$_{2/dppe}$), 1.77 (m, 4H, CH$_{2/Bu}$), 1.60 (s, 30H, C$_5$(CH$_3$)$_5$), 1.10 (m, 4H, CH$_{2/Bu}$), 0.75-0.50 (m, 10H, CH$_{2/Bu}$+CH$_{3/Bu}$). ^{t}BuOK (202 mg, 1.6 mmol, 2.5 eq) in THF (30 mL) was added to this solid. The solution was stirred for 2 h and the solvent was removed. After extraction with toluene and evaporation of the solvent, the solid was washed with pentane (2 × 10 mL) and MeOH (10 mL) at 0 °C, to afford the desired complex **1a** as an orange solid (734 mg, 73 %). Anal. Calc for C$_{97}$H$_{102}$P$_4$Fe$_2$: C, 77.49 H, 6.48; Found: C, 77.51, H 6.86. MS (ESI) m/z calc. for C$_{97}$H$_{102}$P$_4$Fe$_2$ (M$^{+•}$): 1502.5631; found: 1502.5641. IR (KBr, cm^{-1}): ν = 2043 (s, FeC≡C); 1600 (s, C=C$_{Flu}$). Raman (neat, cm^{-1}): ν = 2049 (m, FeC≡C), 1597 (vs, C=C$_{Flu}$). ^{31}P NMR (81 MHz, C$_6$D$_6$): δ = 100.7 (s, P_{dppe}). ^{1}H NMR (200 MHz, C$_6$D$_6$): δ = 8.10 (m, 8H, H_{o-dppe}), 7.53 (d, 2H, $^3J_{H,H}$ = 7.6 Hz, H_{Flu}), 7.30-6.95 (m, 36H, H_{Flu} and H_{dppe}), 2.68 (m, 4H, $H_{CH2/dppe}$), 2.05 (m, 4H, CH$_{2-Bu}$), 1.82 (m, 4H, $H_{CH2/dppe}$), 1.57 (s, 30H, C$_5$(CH$_3$)$_5$), 1.19 (m, 4H, CH$_{2/Bu}$), 1.03 (m, 4H, CH$_{2/Bu}$), 0.70 (t, 6H, $^3J_{H,H}$ = 6.8 Hz, CH$_{3/Bu}$). ^{13}C{^{1}H} NMR (125 MHz, C$_6$D$_6$): δ = 151.4 (s, C_{Flu}), 140.8 & 138.8 (m, $C_{Ph-dppe}$), 138.1 (s, C_{Flu}), 136.9 (t, $^2J_{C,P}$ = 40 Hz, FeC≡C), 135.5 & 135.1 (m, $C_{Ph/dppe}$), 130.2 (s, C_{Flu}), 130.0 (s, CH_{Flu}), 129.8 & 129.6 (s, $C_{Ph-dppe}$), 128.1 (m, $C_{Ph/dppe}$), 125.5 (m, CH_{Flu}), 122.6 (s, FeC≡C), 119.8 (s, CH_{Flu}), 88.5 (s, C$_5$(CH$_3$)$_5$), 55.3 (s, C_{Flu}), 41.7 (s, CH$_{2-Bu}$), 31.8 (m, CH$_{2/dppe}$), 28.5 (s, CH$_{2/Bu}$), 24.4 (s, CH$_{2/Bu}$), 14.8 (s, CH$_{3/Bu}$), 11.2 (s, C$_5$(CH$_3$)$_5$).

(NB. Possible ^{13}C NMR assignment as deduced from corresponding mononuclear complex).

Synthesis of Fe(η^5-C$_5$Me$_5$)(κ^2-dppe){C≡C(1,4-C$_6$H$_4$)C≡C-(2,7-C$_{13}$H$_6$/Bu$_2$)C≡C(1,4-C$_6$H$_4$)C≡C}Fe(η^5-C$_5$Me$_5$)(κ^2-dppe) (1b). Fe(η^5-C$_5$Me$_5$)(κ^2-dppe)Cl (**6**; 648 mg, 1.0 mmol, 2.1 eq), 2,7-bis[(4-ethynylphenyl)ethynyl]-9,9-dibutyl-9H-fluorene (**5b'**; 260 mg, 0.49 mmol, 1.0 eq) and KPF$_6$ (191 mg, 1.0 mmol, 2.1 eq) were dissolved in a MeOH/THF (1 : 1) mixture (30 mL) in a Schlenk tube under argon. The solution was stirred and heated at 45 °C for 12 h. The

solvents were removed and the solid was quickly washed with cooled MeOH and extracted with CH_2Cl_2. The solvent was removed and ^tBuOK (135 mg, 1.2 mmol, 2.4 eq) in THF was added under argon. The solution was stirred for 5 h and the solvent was removed. After extraction with toluene and partial evaporation of this solvent, the solid was precipitated and washed with cooled n-pentane to afford the title complex **1b** as an orange solid (543 mg, 64 %). A sample for elemental analysis was reprecipitated from chloroform/n-pentane mixtures. Anal. Calc for $C_{113}H_{110}P_4Fe_2 \cdot CHCl_3$: C, 75.11 H, 6.14; Found: C, 75.10, H 6.32. MS (ESI) m/z 851.3129 ($M^{2+\bullet\bullet}$) calc. for $C_{113}H_{110}P_4Fe_2$: 851.3129 (M^{2+}). FT-IR (KBr, cm^{-1}): ν = 2191 (w, C≡C), 2044 (s, FeC≡C), 1589 (m, $C=C_{Ar}$). Raman (neat, cm^{-1}): ν = 2220 (m, sh), 2199 (m, C≡C), 2047 (m, FeC≡C), 1608 (s, $C=C_{Flu}$), 1592 (vs, $C=C_{Ar}$). $^{31}P\{^1H\}$ NMR (81 MHz, C_6D_6): 101.3 (s, P_{dppe}). ^1H NMR (200 MHz, C_6D_6): δ = 7.95 (m, 8H, $H_{Ph\text{-}dppe}$), 7.69 (s, 2H, H_{12}), 7.59 (m, 8H, H_{Ph}), 7.30 (m, 13H, $H_{Ar}+CHCl_3$), 7.2-6.94 (m, 24H, H_{Ar}), 2.52 (m, 4H, $CH_{2\text{-}dppe}$), 1.84 (m, 8H, $CH_{2/Bu} + CH_{2/dppe}$), 1.52 (s, 15H, $C_5(CH_3)_5$), 0.99 (m, 4H, $CH_{2/Bu}$), 0.73 (m, 4H, $CH_{2/Bu}$), 0.58 (t, $^3J_{H,H}$ = 7.1 Hz, 6H, $CH_{3/Bu}$). $^{13}C\{^1H\}$ NMR (125 MHz, C_6D_6): δ = 152.1 (s, C_{Flu}), 147.3 (t, $^2J_{C,P}$ = 37 Hz, FeC≡C), 141.4 (s, C_{Flu}), 140.0 & 138.6 (2m, $C_{Ph\text{-}dppe}$), 135.2 & 135.0 (2m, $C_{Ph\text{-}dppe}$), 133.8 (s, CH_{Flu}), 132.9 & 131.0 (2s, CH_{Ph}), 130.0 & 129.9 (2s, $C_{Ph\text{-}dppe}$), 128.2 (m, $C_{Ph/dppe}$), 126.3 (s, CH_{Flu}), 124.0 (s, C_{Ph}), 122.1 (broad s, FeC≡C), 120.9 (s, CH_{Flu}), 117.8 (s, C_{Flu}), 92.6 (s, C≡C), 91.7 (s, C≡C), 88.8 (s, $C_5(CH_3)_5$), 56.1 (s, C_{Flu}), 41.2 (s, $CH_{2/Bu}$), 31.5 ($CH_{2/dppe}$), 27.0 (s, $CH_{2/Bu}$), 24.1 (s, $CH_{2/Bu}$), 14.6 (s, CH_3), 11.0 (s, $C_5(CH_3)_5$) [1 C_{Ph} not detected, $C_{1/4}$].

Synthesis of Fe(η^5-C_5Me_5)(κ^2-dppe){C≡C(2-$C_{13}H_7$/Bu$_2$)} (2a). Fe(η^5-C_5Me_5)(κ^2-dppe)Cl (**6**; 517 mg, 0.83 mmol, 1.0 eq), 2-ethynyl-9,9-dibutyl-9H-fluorene (**7a'**; 250 mg, 0.83 mmol, 1.0 eq) and KPF_6 (168 mg, 0.91 mmol, 1.1 eq) were dissolved in MeOH (30 mL) in a Schlenk tube. The solution was heated to 35 °C and stirred at this temperature for 12 h. The brown suspension was allowed to settle and filtered. This solid, which was washed with MeOH (10 mL) at 0 °C

and dried under vacuum, corresponds to the vinylidene complex [Fe(η^5-C_5Me_5)(κ^2-dppe){C=CH(2-$C_{13}H_7$/Bu$_2$)}][PF$_6$] (**2a-v**[PF$_6$]). IR (KBr, cm^{-1}): ν = 1623 (s, Fe=C=C), 1601 (s, $C=C_{Flu}$), 840 (vs, PF_6^-). ^{31}P NMR (81 MHz, CDCl$_3$): δ = 89.2 (s, P_{dppe}), -143.1 (hept, $^1J_{P,F}$ = 712 Hz, PF_6^-). ^1H NMR (200 MHz, CDCl$_3$): δ = 7.62-7.10 (m, 25H, H_{Flu} and H_{dppe}), 6.58 (s, 1H, H_{Flu}), 6.29 (d, 1H, $^3J_{H,H}$ = 8 Hz, H_{Flu}), 5.31 (m, 1H, =CH), 3.13 (m, 2H, $CH_{2/dppe}$), 2.57 (m, 2H, $CH_{2/dppe}$), 1.90 (m, 4H, $CH_{2/Bu}$), 1.64 (s, 15H, $C_5(CH_3)_5$), 1.10 (m, 4H, $CH_{2/Bu}$), 0.75-0.60 (m, 10H, $CH_{2/Bu}$ & $CH_{3/Bu}$). ^tBuOK (113 mg, 0.91 mg, 1.1 eq) and THF (30 mL) were then added. The solution was stirred for 2 h and the solvent was removed. After extraction with toluene and evaporation of the solvent, the solid was washed with pentane (2 × 10 mL) and MeOH (10 mL) at 0 °C, to afford the title complex **2a** as an orange solid (388 mg, 53 %). Crystals were obtained by vapor diffusion of n-pentane into a benzene solution of the compound. Anal. Calc for $C_{59}H_{64}P_2Fe$: C, 79.54; H, 7.24; Found: C, 79.31; H, 7.26. MS (ESI) m/z 890.3837 ($M^{+\bullet}$) calc. for $C_{59}H_{64}P_2Fe$: 890.3833 ($M^{+\bullet}$). FT-IR (KBr, cm^{-1}): ν = 2049 (s, C≡C); 1598 (m, $C=C_{Flu}$). Raman (neat, cm^{-1}): ν = 2051 (s, FeC≡C), 1600 (vs, $C=C_{Flu}$). $^{31}P\{^1H\}$ NMR (81 MHz, C_6D_6): δ = 101.6 (s, (dppe)Fe). ^1H NMR (300 MHz, C_6D_6): δ = 8.19 (m, 4H, $H_{Ph\text{-}dppe}$), 7.66 (2×d, $^3J_{H,H}$ ≈ 7.6 Hz, 2H, 2×$H_{4/5}$), 7.47-7.42 (m, 10H, $H_{Ph\text{-}dppe}$), 7.40 (m, 1H, H_3), 7.36 (m, 1H, H_8), 7.33 (s, 1H, H_1), 7.32 (m, 1H, H_6), 7.28 (m, 1H, H_7), 7.28-7.15 (m, 6H, $H_{Ph/dppe}$), 2.77 (m, 2H, $CH_{2/dppe}$), 2.14 (t, $^3J_{H,H}$ = 7.8 Hz, 4H, $CH_{2/Bu}$, C_{14}), 1.94 (m, 2H, $CH_{2/dppe}$), 1.56 (s, 15H, $C_5(CH_3)_5$), 1.24 (m, 4H, $CH_{2\text{-}Bu}$, C_{15}), 0.99 (m, 4H, $CH_{2\text{-}Bu}$, C_{16}), 0.77 (t, $^3J_{H,H}$ = 7.2 Hz, 6H, CH_3, C_{17}). $^{13}C\{^1H\}$ NMR (75 MHz, C_6D_6): δ = 151.6 & 151.4 (s, C_{Flu}), 143.1 (s, C_{Flu}), 140.5 (m, $C_{Ph/dppe}$), 139.4 (t, $^3J_{C,P}$ = 39.2 Hz, FeC≡C), 138.8 (m, $C_{Ph/dppe}$), 137.3 (s, C_{Flu}), 135.5 & 135.1 (m, $CH_{Ph/dppe}$), 131.5 (s, C_{Flu}), 130.1 (s, CH_{Flu}), 129.9 & 129.8 (s, $CH_{Ph/dppe}$), 128.2 (s, $CH_{Ph/dppe}$), 127.8 (s, CH_{Flu}), 126.8 (s, CH_{Flu}), 125.5 (s, CH_{Flu}), 123.6 (s, CH_{Flu}), 122.5 (s, FeC≡C), 120.5 (s, CH_{Flu}), 120.1 (s, CH_{Flu}), 88.5 (s, $C_5(CH_3)_5$), 55.6 (s, C_{Flu}), 41.6 (s, $CH_{2/Bu}$), 31.8 (m, $CH_{2/dppe}$), 27.2 (s, $CH_{2\text{-}Bu}$), 24.3 (s, $CH_{2/Bu}$), 14.8 (s, CH_3), 11.2 (s, $C_5(CH_3)_5$).

Synthesis of Fe(η^5-C$_5$Me$_5$)(κ^2-dppe){C≡C(1,4-C$_6$H$_4$)C≡C(2-C$_{13}$H$_7$/Bu$_2$)} (2b). Fe(η^5-C$_5$Me$_5$)(κ^2-dppe)Cl (**6**; 330 mg, 0.5 mmol, 1 eq), 2-(4-ethynylphenyl)ethynyl-9,9-dibutyl-9-*H*-fluorene (**7b'**; 213 mg, 0.49 mmol, 1.0 eq) and KPF$_6$ (191 mg, 1.0 mmol, 2.0 eq) were dissolved in a 30 mL mixture of MeOH/THF (1 :1) in a Schlenk tube under argon. The solution was stirred and heated at 45 °C for 12 h. The solvents were removed and the solid was quickly washed with cooled MeOH and extracted with dichloromethane. The solvent was removed and ^{t}BuOK (135 mg, 1.2 mmol, 2.4 eq) in THF was added. The solution was stirred for 5 h and the solvent was removed. After extraction with toluene and partial evaporation of this solvent, the solid was precipitated and then washed with cooled *n*-pentane, to afford the title complex **2b** as an orange solid (543 mg, 64 %). Crystals were obtained by vapor diffusion of methanol into a toluene solution of the compound. Anal. Calc for C$_{67}$H$_{68}$P$_2$Fe: C, 81.20; H, 6.92; Found : C, 81.20; H, 6.96. MS (ESI) m/z 990.4144 (M$^{+•}$) calc. for C$_{67}$H$_{68}$P$_2$Fe: 990.4146. FT-IR (KBr, cm^{-1}): ν = 2193 (w, C≡C), 2047 (s, FeC≡C), 1608 (m, C=C$_{Flu}$), 1589 (s, C=C$_{Ar}$). Raman (neat, cm^{-1}): ν = 2215 (sh, C≡C), 2198 (m, C≡C), 2045 (m, FeC≡C), 1591 (vs, C=C$_{Ar}$). ^{31}P{^{1}H} NMR (81 MHz, C$_6$D$_6$): δ = 101.3 (s, P_{dppe}). ^{1}H NMR (400 MHz, C$_6$D$_6$): δ = 7.96 (m, 4H, $H_{Ph/dppe}$), 7.73 (s, 1H, H$_{18}$), 7.60 (m, 3H, H$_{2/3}$+H$_{8/9}$), 7.52 (m, 1H, H_{Flu}), 7.43 (d, $^3J_{H,H}$ = 7.8 Hz, 1H, H$_{Flu}$), 7.64-7.03 (m, 21H, H_{Ar}), 2.61 (m, 4H, C$H_{2\text{-dppe}}$), 1.91 (m, 8H, C$H_{2/Bu}$+ C$H_{2\text{-dppe}}$), 1.53 (s, 15H, C$_5$(CH_3)$_5$), 0.99 (m, 4H, C$H_{2/Bu}$), 0.71 (m, 4H, C$H_{2/Bu}$), 0.60 (t, $^3J_{H,H}$ = 7.1 Hz, 6H, CH_3). ^{13}C{^{1}H} NMR (125 MHz, C$_6$D$_6$): δ = 152.0 (s, C_{Flu}), 151.8 (s, C_{Flu}), 145.2 (t, $^2J_{C,P}$ = 39 Hz, FeC≡C), 141.9 (s, C_{Flu}), 141.9 (s, C_{Flu}), 140.2 & 138.4 (2m, C$H_{Ar/dppe}$), 135.2 & 135.0 (2m, C$H_{Ar/dppe}$), 132.5 (s, CH_{Ph}), 131.7 (s, CH_{Flu}), 131.2 (s, CH_{Ph}), 129.8 & 129.6 (2s, C$H_{Ar/dppe}$), 129.6 (s, CH_{Flu}), 128.2 (m, C$H_{Ar/dppe}$), 127.9 (s, CH_{Flu}), 126.9 (s, CH_{Flu}), 124.0 (s, C_{Flu}), 123.7 (s, CH_{Flu}), 122.3 (broad s, FeC≡C), 121.0 (s, CH_{Flu}), 120.8 (s, CH_{Flu}), 118.3 (s, C_{Ph}), 92.7 (s, C≡C), 92.0 (s, C≡C), 88.7 (s, C$_5$(CH$_3$)$_5$), 56.0 (s, C_{Flu}), 41.2 (s, CH$_{2/Bu}$), 31.7 (C$H_{2/dppe}$), 27.0 (s, C$H_{2\text{-Bu}}$), 24.1 (s, C$H_{2\text{-Bu}}$), 14.6 (s, CH_3), 11.1 (s, C$_5$(CH_3)$_5$) [1 C_{Ph} not detected, C$_{1/4}$].

Synthesis of [Fe(η^5-C$_5$Me$_5$)(κ^2-dppe)C≡C(2,7-C$_{13}$H$_6$/Bu$_2$)-C≡CFe(η^5-C$_5$Me$_5$)(κ^2-dppe)][PF$_6$]$_2$ (1a[PF$_6$]$_2$). Fe(η^5-C$_5$Me$_5$)(κ^2-dppe)C≡C(2,7-C$_{13}$H$_6$/Bu$_2$)C≡CFe(η^5-C$_5$Me$_5$)(κ^2-dppe) (**1a**; 200 mg, 0.13 mmol) and [(η^5-C$_5$H$_5$)$_2$Fe][PF$_6$] (88 mg, 0.27 mmol, 2.0 eq) were dissolved in CH$_2$Cl$_2$ (15 mL) in a Schlenk tube, and the solution was stirred for 2 h. After partial removal of the solvent (to *ca.* 5 mL), pentane (60 mL) was added and the solvents were filtered. The residue was then washed with thoroughly deoxygenated toluene (2 × 2 mL) and pentane (2 mL) at 0 °C to obtain the title dication (**1a[PF$_6$]$_2$**) as a dark green solid (188 mg, 80 %). IR (KBr, cm^{-1}): ν = 1980 (s, FeC≡C), 1585 (w, C=C$_{Ar}$), 839 (vs, PF$_6^-$). ^{1}H NMR (200 MHz, CD$_2$Cl$_2$): δ = 17.4 (m, 2H, H_{Ph}), 7.9 (s, 4H, $H_{Ph/dppe}$), 7.3 (m, 8H, $H_{Ph/dppe}$), 6.8 (s, 8H, $H_{Ph/dppe}$), 6.5 (s, 4H, $H_{Ph/dppe}$), 4.2 (m, 8H, $H_{Ph/dppe}$), 2.4-0.0 (m, 26 H, C$H_{n/Bu}$ + $H_{Ph/dppe}$), -2.0 (m, 4H, C$H_{2/Bu}$), -8.7 (s, 30H, C$_5$(CH_3)$_5$), -33.7 (broad s, 2H, CH_{Ph}), -38.1 (broad s, 2H, CH_{Ph}).

Synthesis of [Fe(η^5-C$_5$Me$_5$)(κ^2-dppe){C≡C(1,4-C$_6$H$_4$)C≡C-(2,7-C$_{21}$H$_{24}$)C≡C(1,4-C$_6$H$_4$)C≡C}Fe(η^5-C$_5$Me$_5$)(κ^2-dppe)][PF$_6$]$_2$ (1b[PF$_6$]$_2$). **1b** (150 mg, 0.09 mmol, 1.0 eq) and 58 mg [Fe(η^5-C$_5$H$_5$)$_2$][PF$_6$] (0.18 mmol, 2.0 eq) were dissolved in deoxygenated CH$_2$Cl$_2$ (15 mL) in a Schlenk tube, and the solution was stirred for 1 h. After partial removal of the solvent, the residue was precipitated and washed with cooled toluene (2 × 2 mL) and *n*-pentane (2 × 2 mL), to obtain the title dication **1b[PF$_6$]$_2$** as a green solid (100 mg, 56 %). IR (KBr, cm^{-1}): ν = 2191 (w, C≡C), 1988 (s, FeC≡C), 1583 (m, Ar). ^{1}H NMR (200 MHz, CD$_2$Cl$_2$): δ = 32.1 (4H, C$H_{Ph/dppe}$), 8.6 (d, $^3J_{H,H}$ = 7.7 H, 2H, H_{Flu}), 7.9 (broad s, 4H, $H_{Ph/dppe}$), 7.6 (broad m, >2H, C$H_{2/dppe}$), 7.2 (m, 8H, $H_{Ph/dppe}$), 6.9 (s, 8H, $H_{Ph/dppe}$), 6.3 (s, 4H, $H_{Ph/dppe}$), 3.9 (s, 2H, H_{Flu}), 3.7 (s, 10H, H_{Flu} + $H_{Ph/dppe}$), 2.1-0.8 (m, 26 H, C$H_{n/Bu}$ + $H_{Ph/dppe}$), -2.8 (s, 4H, C$H_{2/dppe}$), -10.4 (s, 30H, C$_5$(CH_3)$_5$), -43.8 (4H, $H_{Ph/dppe}$).

Synthesis of [Fe(η^5-C$_5$Me$_5$)(κ^2-dppe){C≡C(2-C$_{13}$H$_7$/Bu$_2$)}][PF$_6$] (2a[PF$_6$]). **2a** (250 mg, 0.28 mmol, 1.0 eq) and [Fe(η^5-

$C_5H_5)_2][PF_6]$ (88 mg, 0.27 mg, 0.95 eq) were stirred in CH_2Cl_2 (15 mL) for 2 h at 25 °C in a Schlenk tube. After partial removal of the solvent (ca. 5 mL), pentane was added (60 mL) and the solvents were filtered. The residue was then washed with thoroughly deoxygenated toluene (2 mL) and pentane (2 mL) at 0 °C, to obtain the title complex **2a**[PF_6] as a green solid (187 mg, 67 %). MS (ESI) m/z 890.3836 ($M^{+\bullet}$) calc. for $C_{56}H_{64}P_2Fe$: 890.3833 ($M^{+\bullet}$). IR (KBr, cm^{-1}): v = 1989 (m, $FeC\equiv C$), 1595 (w, $C=C_{Ar}$), 839 (vs, PF_6^-). ^1H NMR (200 MHz, CD_2Cl_2): δ = 32.6 (m, 1H, CH_{Flu}), 12.6 (s, 1H, CH_{Flu}), 11.9 (s, 1H, CH_{Flu}), 8.0 (m, 2H, $H_{Ph/dppe}$), 6.7 (m, 4H, $H_{Ph/dppe}$), 6.4 (m, 2H, $H_{Ph/dppe}$), 3.8 (m, 4H, $H_{Ph/dppe}$), 2.8-0.0 (m, 22H, $CH_{n/Bu}$ + $H_{Ph/dppe}$), -3.2 (m, 2H, $CH_{2/dppe}$), -6.6 (m, 1H, CH_{Flu}), -9.0 (m, 1H, CH_{Flu}), -10.2 (s, 15H, $C_5(CH_3)_5$), -49.2 (broad s, 1H, CH_{Ph}), -53.5 (broad s, 1H, CH_{Ph}).

Synthesis of [Fe(η^5-C_5Me_5)(κ^2-dppe){C≡C(1,4-C_6H_4)C≡C-(2-$C_{13}H_7$/Bu_2)}][PF_6] (2b[PF_6]). 2b (150 mg, 0.15 mmol, 1.0 eq) and [Fe(η^5-$C_5H_5)_2][PF_6]$ (47 mg, 0.14 mmol, 0.95 eq) were stirred in CH_2Cl_2 (15 mL) for 1 h at 25 °C in a Schlenk tube. After partial removal of the solvent, the residue was washed with cooled and deoxygenated toluene (2 × 2 mL) and *n*-pentane (2 mL), to obtain the title complex **2b**[PF_6] as a green solid (70 mg, 41 %). IR (KBr, cm^{-1}): v = 2193 (w, C≡C), 1989 (w, $FeC\equiv C$), 1585 (m, $C=C_{Ar}$). ^1H NMR (200 MHz, CD_2Cl_2): δ = 32.4 (s, 2H, CH_{Ph}), 9.7 (broad d, H_{Flu}, $J_{H,H}$ ~ 3.8 Hz), 7.8 (s), 7.7 (s), 7.5 (m), 7.2 (s), 6.9 (s), 6.3 (s), 3.9 (s), 3.7 (s), 3.5 (s), 3.2 (s), 2.1-0.8 (m, $CH_{n/Bu}$ + $H_{Ph/dppe}$ + H_{Flu}), -2.9 (s, 2H, $CH_{2/dppe}$), -10.4 (s, 15H, $C_5(CH_3)_5$), -44.3 (broad s, 2H, CH_{Ph}).

Luminescence Measurements. Luminescence measurements in solution were performed in dilute deoxygenated solutions (except in the case of ligands **5a'**, **5b'**, **8** and **9**) contained in air-tight quartz cells of 1 cm pathlength (ca. 10^{-6} M, optical density < 0.1) at room temperature (298 K), using an Edinburgh Instruments (FLS920) spectrometer equipped with a 450 W Xenon lamp and a Peltier-cooled Hamamatsu R928P photomultiplier tube in photon-counting mode. Fully corrected excitation and emission spectra were obtained with an optical density at $\lambda_{exc} \leq 0.1$ to minimize internal absorption. Luminescence quantum yields were measured according to literature procedures.[69] UV-vis absorption spectra used for the calculation of the luminescence quantum yields were recorded using a double beam Jasco V-570 spectrometer.

DFT Calculations. Calculations were performed using the Amsterdam Density Functional (ADF) program,[70] version ADF2012. Scalar relativistic effects were treated via the Zeroth-Order Regular Approximation (ZORA) method.[71] In all calculations, all-electron Triple Zeta plus Polarization (TZP) Slater orbital basis sets were used for all atoms. Geometry optimizations were undertaken with suitable symmetry constraints using the exchange-correlation (XC) functional and the Generalized Gradient Approximation (GGA) proposed by Becke and Perdew (BP).[72] The model systems were simplified by using 1,2-bis(dimethylphosphino)-methane (dmpm) ligands instead of 1,2-bis(diphenyl-phosphino)ethane (dppe) and methyls instead of the butyl groups. UV-Vis spectra were calculated using the Statistical Average of Orbital Potentials (SAOP) functional[73] with the same TZP basis sets.

Z-scan Measurements. Third-order nonlinear optical properties were investigated as previously described,[74] but with some modifications. The laser system consisted of a Quantronix Integra-C3.5F pumping a Quantronix Palitra-FS optical parametric amplifier, tuneable over a wavelength range from 500 nm to 2000 nm. The output wavelength was confirmed by use of an Ocean Optics USB2000+ spectrometer (500-1000 nm) or an Ocean Optics NIR-Quest spectrometer (1000-1800 nm). The system delivered 130 fs pulse with a 1 kHz repetition rate. Colored glass filters and a Thorlabs polarizing filter were used to remove unwanted wavelengths and the power adjusted by use of neutral density filters, attenuating it to the μJ/pulse range to obtain nonlinear phase shifts between 0.2 to 1.3 rad. The focal length of the lens used in the experiment was 75 mm, which gave 25-40 μm

beam waists resulting in Rayleigh lengths sufficiently longer than that of the sample thickness that a "thin-sample" assumption was justified. Solutions of compounds in "as received" CH_2Cl_2 (see text), deoxygenated and distilled CH_2Cl_2, or deoxygenated and distilled THF, of 0.1 w/w% concentration in 1 mm glass cells were analyzed. Samples travelled down the Z-axis on a Thorlabs motorized stage between -20 and 20 mm (where 0 was the laser focus). Data were collected by three Thorlabs photodiodes, 500-900 nm with Si based detectors, 900-1300 nm with InGaAs detectors and 1300-2000 nm with amplified InGaAs detectors, monitoring the laser input, the open-aperture signal and the closed-aperture signal. Data from the detectors were fed into three channels of a Tektronix digital oscilloscope, collected with a custom LabVIEW program, and fitted with theoretical traces with a program that used equations derived by Sheik-Bahae *et al.*[73] A sample of the solvent was run at each wavelength to account for solvent and cell contribution to the Z-scan signals, and the light intensity was determined from a Z-scan run on a 3 mm fused silica plate; the real and imaginary components of the second hyperpolarizability (γ) of the materials were calculated assuming additivity of the nonlinear contributions of the solvent and the solute and the applicability of the Lorentz local field approximation. The values of the imaginary parts of γ were also converted into values of the two-photon absorption cross-sections σ_2.

Crystallography. Data collection of crystals of $\mathbf{1a \cdot C_6H_6}$, $\mathbf{2a}$ and $\mathbf{2b \cdot C_7H_8}$ was performed on an Oxford Diffraction Xcalibur Sapphire 3 diffractometer at 110 K, 130 K and 150 K, respectively, with graphite monochromated MoK_α radiation. The cell parameters (Supporting Information) were obtained with Denzo and Scalepack.[75] The data collection[76] provided reflections from which the independent reflections were obtained after data reduction using Denzo and Scalepack.[75] The structures were solved with SIR-97 which revealed the non-hydrogen atoms.[77] After anisotropic refinement, the remaining atoms were found in Fourier difference maps. The complete structures were then refined with SHELXL97[78] by the full-matrix least-square technique.

Atomic scattering factors were taken from the literature.[79] ORTEP views of $\mathbf{1a}$, $\mathbf{2a}$ and $\mathbf{2b}$ were generated with PLATON98.[80]

ASSOCIATED CONTENT

Supporting Information

Synthesis and characterization of $\mathbf{5a'\text{-}b'}$ and $\mathbf{7a'\text{-}b'}$. ^{1}H NMR spectra of $\mathbf{1b}[PF_6]_2$ and $\mathbf{2b}[PF_6]$ and magnetic measurements on $\mathbf{1a}[PF_6]_2$. Fitting of the IVCT band of $\mathbf{1a}[PF_6]$ in acetone. Crystallographic (CIF files), computational (Cartesian coordinates) data and Z-scan data on the complexes. CIF files for $\mathbf{1a}$, $\mathbf{2a}$ and $\mathbf{2b}$ have been deposited at the Cambridge Crystallographic Data Center and were allocated the deposition numbers CCDC 691930, CCDC 694575 and CCDC 776248, respectively. Ordering information is given on any current masthead page.

AUTHOR INFORMATION

Corresponding Authors

frederic.paul@univ-rennes1.fr
Tel: (+33) 02 23 23 59 62; Fax: (+33) 02 23 23 56 37.
Mark.Humphrey@anu.edu.au
Tel: (+61) 02 61252927; Fax: (+61) 02 61250750.

Notes
The authors declare no competing financial interest.

REFERENCES

(1) Nijegorodov, N. I.; Downey, W. S. *J. Phys. Chem.* **1994**, *98*, 5639-5643.

(2) Belfield, K. D.; Bondar, M. V.; Hernandez, F. E.; Przhonska, O. V.; Yao, S. *J. Phys. Chem. B* **2007**, *111*, 12723-12729.

(3) See for instance: (a) Yang, R.; Xu, Y.; Dang, X.-D.; Nguyen, T.-Q.; Cao, Y.; Bazan, G. C. *J. Am. Chem. Soc.* **2008**, *130*, 3282-3283; (b) Ranger, M.; Leclerc, M. *Macromolecules* **1999**, *32*, 3306-3313.

(4) Hapiot, P.; Lagrost, C.; Le Floch, F.; Raoult, E.; Rault-Berthelot, J. *Chem. Mater.* **2005**, *17*, 2003-2012.

(5) Poriel, C.; Liang, J.-J.; Rault-Berthelot, J.; Barrière, F.; Cocherel, N.; Slawin, A. M. Z.; Horhant, D.; Virboul, M.; Alcaraz, G.; Audebrand, N.; Vignau, L.; Huby, N.; Wantz, G.; Hirsch, L. *Chem. Eur. J.* **2007**, *13*, 10055 – 10069.

(6) See for instance: (a) Chinelatto, L. S., Jr; del Barrioa, J.; Pinol, M.; Oriol, L.; Matranga, M.A.; Santo, M. P. D.; Barberi, R. *J. Photochem. Photobiol. A: Chemistry* **2010**, *210*, 130-139; (b) Feng, X. J.; Wu, P. L.; Tam, H. L.; Li, K. F.; Wong, M. S.; Cheah, K. W. *Chem. Eur. J.* **2009**, *15*, 11681-11691; (c) Ren, S.; Cheng, J.; Zeng, D.; Zhu, W.; Sun, J.; Du, J.; Xu, E.; Zhong, H.; Liu, Y.; Fang, Q. *Synth. Metals* **2009**, *159*, 29-35.

(7) (a) Grimsdale, A. C.; Müllen, K. *Macromol. Rapid Commun.* **2007**, *28*, 1676-1702; (b) Neher, D. *Macromol. Rapid Commun.* **2001**, *22*, 1365-1385; (c) Wong, W.-Y. *Coord. Chem. Rev.* **2005**, *249*, 971-997.

(8) Silly, M. G.; Porres, L.; Mongin, O.; Chollet, P. A.; Blanchard-Desce, M. *Chem. Phys. Lett.* **2003**, *379*, 74-80.

(9) Liu, R.; Azenkeng, A.; Li, Y.; Sun, W. *Dalton Trans.* **2012**, *41*, 12353-12357.

(10) (a) Mongin, O.; Krishna, T. R.; Werts, M. H. V.; Caminade, A.-M.; Majoral, J.-P.; Blanchard-Desce, M. *Chem. Commun.* **2006**, 915–917; (b) Terenziani, F.; Katan, C.; Badaeva, E.; Tretiak, S.; Blanchard-Desce, M. *Adv. Mater.* **2008**, *20*, 4541-4678; (c) Rouxel, C.; Charlot, M.; Mongin, O.; Krishna, T. R.; Caminade, A.-M.; Majoral, J.-P.; Blanchard-Desce, M. *Chem. Eur. J.* **2012**, *18*, 16450-16462.

(11) Rebane, A.; Drobizhev, M.; Makarov, N. S.; Beuerman, E.; Haley, J. E.; Krein, D. M.; Burke, A. R.; Flikkema, J. L.; Cooper, T. M. *J. Phys. Chem. A* **2011**, *115*, 4255-4262.

(12) Mongin, O.; Porrès, L.; Charlot, M.; Katan, C.; Blanchard-Desce, M. *Chem. Eur. J.* **2007**, *13*, 1481-1498.

(13) Akita, M.; Koike, T. *J. Chem. Soc., Dalton Trans.* **2008**, 3523-3530.

(14) Paul, F.; Lapinte, C. *Coord. Chem. Rev.* **1998**, *178/180*, 431-509.

(15) Ibn Ghazala, S.; Paul, F.; Toupet, L.; Roisnel, T.; Hapiot, P.; Lapinte, C. *J. Am. Chem. Soc.* **2006**, *128*, 2463-2476 and refs therein.

(16) Malvolti, F.; Rouxel, C.; Mongin, O.; Hapiot, P.; Toupet, L.; Blanchard-Desce, M.; Paul, F. *Dalton Trans.* **2011**, *40*, 6616-6618.

(17) (a) Drouet, S.; Merhi, A.; Grelaud, G.; Cifuentes, M. P.; Humphrey, M. G.; Matczyszyn, K.; Samoc, M.; Toupet, L.; Paul-Roth, C. O.; Paul, F. *New J. Chem.* **2012**, *36*, 2192 - 2195; (b) Drouet, S.; Merhi, A.; Yao, D.; Cifuentes, M. P.; Humphrey, M. G.; Wielgus, M.; Olesiak-Banska, J.; Matczyszyn, K.; Samoc, M.; Paul, F.; Paul-Roth, C. O. *Tetrahedron* **2012**, *68*, 10351-10359; (c) Green, K. A.; Simpson, P. V.; Corkery, T. C.; Cifuentes, M. P.; Samoc, M.; Humphrey, M. G. *Macromol. Rapid Commun.* **2012**, *33*, 573–578; (d) Samoc, M.; Corkery, T. C.; McDonagh, A. M.; Cifuentes, M. P.; Humphrey, M. G. *Aust. J. Chem.* **2011**, *64*, 1269-1273; (e) Jeffery, C. J.; Cifuentes, M. P.; Willis, A. C.; Samoc, M.; Humphrey, M. G. *Macromol. Rapid Commun.* **2010**, *31*, 846-849; (f) Roberts, R. L.; Schwich, T.; Corkery, T. C.; Cifuentes, M. P.; Green, K. A.; Farmer, J. D.; Low, P. J.; Marder, T. B.; Samoc, M.; Humphrey, M. G. *Adv. Mat.* **2009**, *21*, 2318-2322; (g) Green, K. A.; Cifuentes, M. P.; Corkery, T. C.; Samoc, M.; Humphrey, M. G. *Angew. Chem., Int. Ed. Engl.* **2009**, *48*, 7867-70; (h) Dalton, G. T.; Cifuentes, M. P.; Watson, L. A.; Petrie, S.; Stranger, R.; Samoc, M.; Humphrey, M. G. *Inorg. Chem.* **2009**, *48*, 6534-6547; (i) Babgi, B.; Rigamonti, L.; Cifuentes, M. P.; Corkery, T. C.; Randles, M. D.; Schwich, T.; Petrie, S.; Stranger, R.; Teshome, A.; Asselberghs, I.; Clays, K.; Samoc, M.; Humphrey, M. G. *J. Am. Chem. Soc.* **2009**, *131*, 10293–10307; (j) Dalton, G. T.; Cifuentes, M. P.; Petrie, S.; Stranger, R.; Humphrey, M. G.; Samoc, M. *J. Am. Chem. Soc.* **2007**, *129*, 11882-11883; (k) Powell, C. E.; Humphrey, M. G. *Coord. Chem. Rev.* **2004**, *248*, 725-756; (l) Powell, C. E.; Morrall, J. P.; Ward, S. A.; Cifuentes, M. P.; Notaras, E. G. A.; Samoc, M.; Humphrey, M. G. *J. Am. Chem. Soc.* **2004**, *126*, 12234-12235.

(18) (a) Morrall, J. P.; Dalton, G. T.; Humphrey, M. G.; Samoc, M. *Adv. Organomet. Chem.* **2008**, *55*, 61-136; (b) Hurst, S. K.; Humphrey, M. G.; Morrall, J. P.; Cifuentes, M. P.; Samoc, M.; Luther-Davies, B.; Heath, G. A.; Willis, A. C. *J. Organomet. Chem.*, **2003**, *670*, 56-65; (c) McDonagh, A. M.; Cifuentes, M. P.; Whittall, I. R.;

Humphrey, M. G.; Samoc, M.; Luther-Davies, B.; Hockless, D. C. R. *J. Organomet. Chem.*, **1996**, *526*, 99-103.

(19) (a) Gauthier, N.; Olivier, C.; Rigaut, S.; Touchard, D.; Roisnel, T.; Humphrey, M. G.; Paul, F. *Organometallics* **2008**, *27*, 1063-1072; (b) Courmarcel, J.; Le Gland, G.; Toupet, L.; Paul, F.; Lapinte, C. *J. Organomet. Chem.* **2003**, *670*, 108-122.

(20) Grelaud, G.; Cifuentes, M. P.; Paul, F.; Humphrey, M. G. *J. Organomet. Chem.* **2014**, *751*, 181-200.

(21) μ_{gg} is the ground state dipole moment, μ_{ee} is an excited state dipole moment, $\mu_{ee'}$ and μ_{ge} are transition dipole moments, and E_{ge} and $E_{ge'}$ are optical absorption energies.

(22) (a) Wong, W.-Y.; Ho, C.-L. *Coord. Chem. Rev.* **2006**, *250*, 2627-2690; (b) Wong, W.-Y. *J. Inorg. Organomet. Polym. Mater.* **2005**, *15*, 197-219.

(23) Lewis, J.; Raithby, P. R.; Wong, W.-Y. *J. Organomet. Chem.* **1998**, *556*, 219-228.

(24) For ferrocene-containing analogues, see: (a) Wong, W.-Y.; Lu, G.-L.; Choi, K.-H.; Guo, Y.-H. *J. Organomet. Chem.* **2005**, *690*, 177-186; (b) Wong, W.-Y.; Lu, G.-L.; Ng, K.-F.; Wong, C.-K.; Choi, K.-H. *J. Organomet. Chem.* **2001**, *637-639*, 159-166.

(25) Denis, R.; Toupet, L.; Paul, F.; Lapinte, C. *Organometallics* **2000**, *19*, 4240-4251.

(26) Khan, M. S.; Al-Mandhary, M. R. A.; Al-Suti, M. K.; Ahrens, B.; Mahon, M. F.; Male, L.; Raithby, P. R.; Boothby, C. E.; Köhler, A. *Dalton Trans.* **2003**, 74-84.

(27) Cifuentes, M. P.; Humphrey, M. G.; Morrall, J. P.; Samoc, M.; Paul, F.; Roisnel, T.; Lapinte, C. *Organometallics* **2005**, *24*, 4280-4288.

(28) Costuas, K.; Paul, F.; Toupet, L.; Halet, J.-F.; Lapinte, C. *Organometallics* **2004**, *23*, 2053-2068.

(29) Paul, F.; Toupet, L.; Thépot, J.-Y.; Costuas, K.; Halet, J.-F.; Lapinte, C. *Organometallics* **2005**, *24*, 5464-5478.

(30) Astruc, D. Electron Transfer and Radical Processes in Transition-Metal Chemistry; VCH Publishers, Inc.: Weinheim, 1995.

(31) Richardson, D. E.; Taube, H. *Coord. Chem. Rev.* **1984**, *60*, 107-129.

(32) Paul, F.; da Costa, G.; Bondon, A.; Gauthier, N.; Sinbandhit, S.; Toupet, L.; Costuas, K.; Halet, J.-F.; Lapinte, C. *Organometallics* **2007**, *26*, 874-896.

(33) Paul, F.; Bondon, A.; da Costa, G.; Malvolti, F.; Sinbandhit, S.; Cador, O.; Costuas, K.; Toupet, L.; Boillot, M.-L. *Inorg. Chem.* **2009**, *48*, 10608–10624.

(34) However, a precise assignment of the H_d/H_f and H_e/H_g pairs of resonances proved experimentally not possible.

(35) A larger negative value can be extracted from the VT-NMR data in CH_2Cl_2 consistently with the mostly intramolecular origin of this interaction, however, the latter value should be considered with extreme care given the small temperature range probed by this technique.[37]

(36) Kahn, O. *Molecular Magnetism*; VCH: Cambridge, 1993.

(37) Paul, F.; Malvolti, F.; da Costa, G.; Stang, S. L.; Justaud, F.; Argouarch, G.; Bondon, A.; Sinbandhit, S.; Costuas, K.; Toupet, L.; Lapinte, C. *Organometallics* **2010**, *29*, 2491–2502.

(38) Aly, S. M.; Ho, C.-L.; Wong, W.-Y.; Fortin, D.; Harvey, P. D. *Macromolecules* **2009**, *42*, 6902-6916.

(39) The emission spectra of the organic fluorene precursors **3a** and **5a** are typical of fluorene-based chromophores, with vibronic progressions of ca. 1460 cm^{-1}, the most intense peaks corresponding to the 0-0 transitions.

(40) Sohn, Y. S.; Hendrickson, D. N.; Gray, H. B. *J. Am Chem. Soc.* **1970**, *93*, 3233-3234.

(41) (a) Paul, F.; Mevellec, J.-Y.; Lapinte, C. *J. Chem. Soc., Dalton Trans.* **2002**, 1783-1790; (b) Le Stang, S.; Paul, F.; Lapinte, C. *Organometallics* **2000**, *19*, 1035-1043.

(42) Brunschwig, B. S.; Creutz, C.; Sutin, N. *Chem. Soc. Rev.* **2002**, *31*, 168-184.

(43) Robin, M. B.; Day, P. *Adv. Inorg. Chem. Radiochem.* **1967**, 247-422.

(44) (a) Chung, M.-I.; Gu, X.; Etzenhouser, B. A.; Spuches, A. M.; Rye, P. T.; Seetharaman, S. K.; Rose, D. J.; Zubieta, J.; Sponsler, M. B. *Organometallics* **2003**, *22*, 3485-3494; (b) Matsuura, Y.; Tanaka, Y.; Akita, M. *J. Organomet. Chem.* **2009**, *694*, 1840-1847.

(45) Demadis, K. D.; Hartshorn, C. M.; Meyer, T. J. *Chem. Rev.* **2001**, *101*, 2655-2685.

(46) Allen, G. C.; Hush, N. S. *Prog. Inorg. Chem.* **1967**, *8*, 357-389.

(47) Hush, N. S. *Prog. Inorg. Chem.* **1967**, *8*, 391-444.

(48) In this solvent a smaller comproportionation constant is expected, since the difference between the oxidation peaks is smaller than in CH_2Cl_2 ($\Delta E^0 = 84$ mV).

(49) For solvent effects on electronic couplings, see also ref. 50.

(50) (a) Lin, Y.-C.; Chen, W.-T.; Tai, J.; Su, D.; Huang, S.-Y.; Lin, I.; Lin, J.-L.; Lee, M. M.; Chiou, M. F.; Liu, Y.-H.; Kwan, K.-S.; Chen, Y.-J.; Chen, H.-Y. *Inorg. Chem.* **2009**, *48*, 1857-1872; (b) Chen, Y. J.; Kao, C.-H.; Lin, S. J.; Tai, C.-C.; Kwan, K. S. *Inorg. Chem.* **2000**, *39*, 189-194.

(51) The IVCT band B, which possesses the correct theoretical bandwith according to eq. 3, would correspond to an electronic coupling of ca. 14 cm^{-1} (eq. 4) for a Fe-Fe distance (d_{FeFe}) of 30 Å. E.g. see for: (a) Wielgus, M.; Bartkowiak, W.; Samoc, M. *Chem. Phys. Lett.* **2012**, *554*, 113-116; (b) Wielgus, M.; Zalesny, R.; Murugan, N.; Kongsted, J.; Ågren, H.; Samoc, M.; Bartkowiak, W. *ChemPhysChem* **2013**, *14*, 3731-3739; (c) Wielgus, M.; Michalska, J.; Samoc, M.; Bartkowiak, W. *Dyes and Pigments* **2014**, *113*, 426-434.

(53) (a) Marvaud, V.; Launay, J.-P.; Joachim, C. *Chem. Phys.* **1993**, *177*, 23-30; (b) Patoux, C.; Coudret, C.; Launay, J.-P.; Joachim, C.; Gourdon, A. *Inorg. Chem.* **1997**, *36*, 5037-5049.

(54) Paddon-Row, M. N. *Adv. Phys. Org. Chem.* **2003**, *38*, 1-85.

(55) Considering a rough doubling of the Fe-Fe distance between **1a**[PF$_6$] to **1b**[PF$_6$] from the X-ray data available and taking the α_{el} coefficient found for polyphenylene spacers (0.2 Å^{-1}), the electronic coupling in **1a**[PF$_6$] (380 cm^{-1}) should drop to ca. 20 cm^{-1} in **1b**[PF$_6$] when obeying a classic exponential decrease (eq. 5).[54]

$$(H_{FeFe})_d = (H_{FeFe})_0\exp(-\alpha_{el}.d_{FeFe}) \qquad (5).$$

(56) D'Amico, C.; Lorenc, M.; Collet, E.; Green, K. A.; Costuas, K.; Mongin, O.; Blanchard-Desce, M.; Paul, F. *J. Phys. Chem. C* **2012**, *116*, 3719-3727.

(57) de Montigny, F.; Argouarch, G.; Roisnel, T.; Toupet, L.; Lapinte, C.; Lam, S. C.-F.; Tao, C.-H.; Yam, V. W.-W. *Organometallics* **2008**, *27*, 1912-1923.

(58) Such an electron-transfer quenching process is, in principle, possible on thermodynamic grounds based on our data and on published reduction potentials for fluorene[5]: $v_{em} \geq 3.2$ eV > 2.8 eV $\geq$ $E°(Fe^{III}/Fe^{II})$-$E°(Flu/Flu^-)$.

(59) (a) Murai, M.; Sugimoto, M.; Akita, M. *Dalton Trans.* **2013**, *42*, 16108–16120; (b) Wong, K. M.-C.; Lam, S. C.-F.; Ko, C.-C.; Zhu, N.; Yam, V. W.-W.; Roué, S.; Lapinte, C.; Fathallah, S.; Costuas, K.; Kahlal, S.; Halet, J.-F. *Inorg. Chem.* **2003**, *42*, 7086-7097.

(60) Powell, C. E.; Cifuentes, M. P.; Morrall, J. P.; Stranger, R.; Humphrey, M. G.; Samoc, M.; Luther-Davies, B.; Heath, G. A. *J. Am. Chem. Soc.* **2003**, *125*, 602-610.

(61) Whittall, I. R.; McDonagh, A. M.; Humphrey, M. G.; Samoc, M. *Adv. Organomet. Chem.* **1999**, *43*, 349-405.

(62) Rogers, J. E.; Slagle, J. E.; Krein, D. M.; Burke, A. R.; Hall, B. C.; Fratini, A.; McLean, D. G.; Fleitz, P. A.; Cooper, T. M.; Drobizhev, M.; Makarov, N. S.; Rebane, A.; Kim, K.-Y.; Farley, R.; Schanze, K. S. *Inorg. Chem.* **2007**, *46*, 6483-6494.

(63) He, G. S.; Tan, L.-S.; Zheng, Q.; Prasad, P. N. *Chem. Rev.* **2008**, *108*, 1245-1330.

(64) Cifuentes, M. P.; Powell, C. E.; Humphrey, M. G.; Heath, G. A.; Samoc, M.; Luther-Davies, B. *J. Phys. Chem. A* **2001**, *105*, 9625-9627.

(65) Gauthier, N.; Argouarch, G.; Paul, F.; Toupet, L.; Ladjarafi, A.; Costuas, K.; Halet, J.-F.; Samoc, M.; Cifuentes, M. P.; Corkery, T. C.; Humphrey, M. G. *Chem. Eur. J.* **2011**, *17*, 5561-5577.

(66) (a) Paul, F.; Ellis, B. J.; Bruce, M. I.; Toupet, L.; Roisnel, T.; Costuas, K.; Halet, J.-F.; Lapinte, C. *Organometallics* **2006**, *25*, 649-665; (b) Bruce, M. I.; Burgun, A.; Gendron, F.; Grelaud, G.; Halet, J.-F.; Skelton, B. W. *Organometallics* **2011**, *30*, 2861-2868.

(67) (a) Zhu, Y.; Guang, S.; Xu, H.; Su, X.; Liu, X. *J. Mater. Chem. C* **2013**, *1*, 5277-5284; (b) Devi, C. L.; Yesudas, K.; Makarov, N. S.; Rao, V. J.; Bhanuprakash, K.; Perry, J. W. *J. Mater. Chem. C* **2015**, *3*, 3730-3744.

(68) Roger, C.; Hamon, P.; Toupet, L.; Rabaâ, H.; Saillard, J.-Y.; Hamon, J.-R.; Lapinte, C. *Organometallics* **1991**, *10*, 1045-1054.

(69) Demas, N.; Crosby, G. A. *J. Phys. Chem.* **1971** *75*, 991-1024; Eaton, D. F. *Pure Appl. Chem.* **1988**, *60*, 1107-1114.

(70) Baerends, E. J.; Ziegler, T.; Autschbach, J.; Bashford, D.; Bérces, A.; Bickelhaupt, F. M.; Bo, C.; Boerrigter, P. M.; Cavallo, L.; Chong, D. P.; Deng, L.; Dickson, R. M.; Ellis, D. E.; van Faassen, M.; Fan, L.; Fischer, T. H.; Fonseca Guerra, C.; Ghysels, A.; Giammona, A.; van Gisbergen, S. J. A.; Götz, A. W.; Groeneveld, J. A.; Gritsenko, O. V.; Grüning, M.; Gusarov, S.; Harris, F. E.; van den Hoek, P.; Jacob, C. R.; Jacobsen, H.; Jensen, L.; Kaminski, J. W.; van Kessel, G.; Kootstra, F.; Kovalenko, A.; Krykunov, M. V.; van Lenthe, E.; McCormack, D. A.; Michalak, A.; Mitoraj, M.; Neugebauer, J.; Nicu, V. P.; Noodleman, L.; Osinga, V. P.; Patchkovskii, S.; Philipsen, P. H. T.; Post, D.; Pye, C. C.; Ravenek, W.; Rodríguez, J. I.; Ros, P.; Schipper, P. R. T.; Schreckenbach, G.; Seldenthuis, J. S.; Seth, M.; Snijders, J. G.; Solà, M.; Swart, M.; Swerhone, D.; te Velde, G.; Vernooijs, P.; Versluis, L.; Visscher, L.; Visser, O.; Wang, F.; Wesolowski, T. A.; van Wezenbeek, E. M.; Wiesenekker, G.; Wolff, S. K.; Woo, T. K.; Yakovlev, A. L.; Amsterdam Density Functional (ADF) program; version 2.3, Vrije Universiteit: Amsterdam, The Netherlands, 2012.

(71) Lenthe, E. V.; Ehlers, A. E.; Baerends, E. J. *J. Chem. Phys.* **1999**, *110*, 8943-8953.

(72) (a) Becke, A. D. *Phys. Rev. A.* **1988**, *38*, 3098-3100; (b) Perdew, J. P. *Phys. Rev. B* **1986**, *33*, 8822-8824; (c) Perdew, J. P. *Phys. Rev. B* **1986**, *34*, 7406.

(73) Gritsenko, O. V.; Schipper, P. R. T.; Baerends, E. J. *Chem. Phys. Lett.* **1999**, *302*, 199-207.

(74) Merhi, A.; Grelaud, G.; Ripoche, N.; Barlow, A.; Cifuentes, M. P.; Humphrey, M. G.; Paul, F.; Paul-Roth, C. O. *Polyhedron* **2015**, *86*, 64-70.

(75) Otwinowski, Z.; Minor, W. In *Methods in Enzymology*; Carter, C. W., Sweet, R. M., Eds.; Academic Press: London, 1997; Vol. 276, p 307-326.

(76) Nonius B. V. *Kappa CCD Software*; Delft: The Netherlands, 1999.

(77) Altomare, A.; Foadi, J.; Giacovazzo, C.; Guagliardi, A.; Moliterni, A. G. G.; Burla, M. C.; Polidori, G. *J. Applied Cryst.* **1998**, *31*, 74-77.

(78) Sheldrick, G. M. *SHELX97-2. Program for the refinement of crystal structures*; Univ. of Göttingen: Germany, 1997.

(79) *International Tables for X-ray Crystallography*; Kynoch Press (present distrib. D. Reidel, Dordrecht): Birmingham, 1974; Vol. IV.

(80) Spek, A. L. *PLATON. A Multipurpose Crystallographic Tool*; Utrecht University: Utrecht, The Netherlands, 1998.
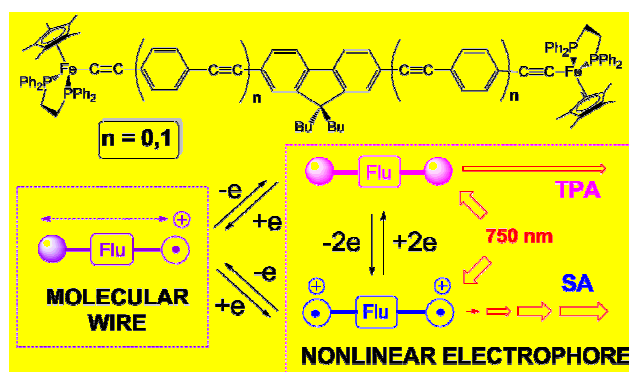
Redox-active organoiron bimetallic complexes containing a 2,7-fluorene unit in the bridge exhibit intramolecular electron-delocalization in their mixed-valent state and switchable cubic nonlinear optical properties. Bridge extension results in less efficient molecular wires, but increasingly contrasted nonlinear electrophores.